Human-Inspired Control of Bipedal Walking Robots

Aaron D. Ames

***Abstract*—This paper presents a *human-inspired control* approach to bipedal robotic walking: utilizing human data and output functions that appear to be intrinsic to human walking in order to formally design controllers that provably result in stable robotic walking. Beginning with human walking data, outputs—or functions of the kinematics—are determined that result in a low-dimensional representation of human locomotion. These same outputs can be considered on a robot, and *human-inspired control* is used to drive the outputs of the robot to the outputs of the human. The main results of this paper are that, in the case of both under and full actuation, the parameters of this controller can be determined through a *human-inspired* optimization that provides the best fit of the human data while simultaneously provably guaranteeing stable robotic walking for which the initial condition can be computed in closed form. These formal results are demonstrated in simulation by considering two bipedal robots—an underactuated 2D bipedal robot, AMBER, and fully actuated 3D bipedal robot NAO—for which stable robotic walking is automatically obtained using only human data. Moreover, in both cases, these simulated walking gaits are realized experimentally to obtain human-inspired bipedal walking on the actual robots.**

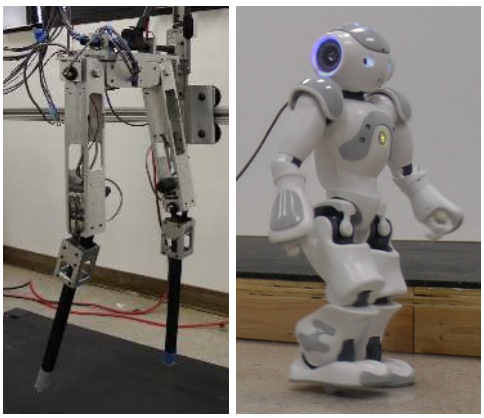

Fig. 1: AMBER, an underactuated 2D bipedal robot, and NAO, a fully actuated 3D bipedal robot.

I. Introduction

Despite the simplicity with which humans appear to walk, human locomotion is inherently complex utilizing hundreds of degrees of freedom coupled with highly nonlinear dynamics and forcing due to the 57 muscles employed during human walking [38]. There is evidence to suggest that humans control walking behaviors through a hierarchical subdivision between cortical control and central pattern generators in the spinal column [10], [15], [18], [26], indicating that when humans perform *motion primitives*, i.e., steady-state well-practiced walking behaviors—potentially simple and characterizable control strategies are implemented. Inspired by this hierarchical control present in humans, the motivation for the ideas presented in this paper is that *the essential information needed to understand walking is encoded by a simple class of functions canonical to human walking*. In other words, taking the control theorist approach to understanding a complex and unknown system, we view the human walking system as a "black box," where the "inputs" to the system are specific walking behaviors, and we seek "outputs" of this system that characterize these behaviors. In this fashion, a low dimensional characterization of the system is achieved. These outputs can then be utilized in the formal design of robotic controllers—the outputs of the robot can be driven to the outputs of the human, resulting in "human-like" robotic walking.

Given human walking as the motivation for achieving robotic walking, this paper begins by looking at human walking data achieved through motion capture of subjects walking on flat ground at a "natural" pace. By studying this data, we discover a collection of *human outputs*, e.g., the forward position of the hip, that appear to characterize human walking—they are mutually exclusive, thus providing a low dimensional representation of the system's behavior. Moreover, we find that these human outputs, as computed from the data, appear to be described by two very simple functions: (i) a linear function of time (describing the forward position of the hip) and (ii) the time solution to a linear spring-mass-damper system (describing the remaining the outputs). We term (ii) *canonical walking functions*, due to their simple yet general form, and verify that in fact these functions describe the human data by showing that they can be fit to the output data with a remarkably high correlation coefficient of essentially 1. This result both motivates the introduction of the general notion of a human output combination, and provides insight into the basic mechanisms underlying human walking since we conclude that, at the most basic level, the primary outputs associated with locomotion are characterized by a system of linear springs and dampers parameterized in time by the forward hip (or walking) velocity.

Utilizing human outputs and their time based representation given by the canonical walking functions, we construct *human-inspired* controllers that drive the outputs of the robot to the outputs of the human as represented by the canonical walking functions. As a specific example, this paper considers a 5 degree of freedom 2D bipedal robot with knees and a torso, for which we define *human-inspired outputs*: the difference between the outputs of the robot (computed via kinematics) and the human outputs (encoded through canonical walking functions parameterized by the forward position of the hip). In the context of both under and full actuation, human-inspired outputs are used to construct *human-inspired controllers* through the use of input-output linearization that drive the human-inspired outputs to zero exponentially fast. Thus, on the corresponding zero dynamics surface, the outputs of the robot and human are in agreement. Since a bipedal robot is a hybrid system (due to the impacts that occur at foot strike), the key challenge is to determine parameters of the human-inspired controller that result in a *hybrid* zero dynamics surface yielding stable robotic walking for which the canonical walking functions best fit the human output data.

The main contribution of this paper is a formal method for determining the parameters of the human-inspired controller that provably results in stable robotic walking that is as "human-like" as possible. Beginning with the case of full actuation, we introduce a *human-inspired* optimization problem where the cost is the least squares fit of the outputs of the robot to the human output data

A. D. Ames is with the Department of Mechanical Engineering, with a joint appointment in Electrical and Computer Engineering, Texas A&M University, College Station TX, 77840 USA, e-mail: aames@tamu.edu.

This research is supported by NSF grants CNS-0953823 and CNS-1136104 and NHARP award 00512-0184-2009.

subject to constraints that ensure *partial hybrid zero dynamics*, i.e., constraints that ensure that the zero dynamics surface associated with the relative degree 2 output functions are invariant through impact. This invariance allows us to characterize the behavior of the hybrid system modeling a bipedal robot (which is 10-dimensional for the examples considered) through a 2-dimensional hybrid system. Utilizing this reduced dimensional representation, we are able to prove the main result of this paper: the parameters that solve the partial human-inspired optimization problem imply the existence of an exponentially stable hybrid periodic orbit, i.e., the existence of stable walking gait. Moreover, the fixed point of the Poincaré map associated with this periodic orbit can be explicitly computed from these parameters. In addition, these results are extended to the case of underactuation, where additional constraints to the human-inspired optimization are added that ensure stable robotic walking, again allowing for the fixed point to be computed in closed form. Therefore, in the case of both under and full actuation, using only the human data we are able to automatically generate parameters for the human-inspired controller that imply the existence of a stable walking gait, and we can explicitly compute the initial condition to this walking gait from these parameters in the case of both full and under actuation.

To demonstrate the validity of the formal methods employed in this paper, we apply them to two bipedal robots (shown in Fig. 1): AMBER, an underactuated 2D bipedal robot, and NAO, a fully actuated 3D bipedal robot for which we consider a simplified 2D sagittal representation. In both cases, we apply the constructions of this paper to automatically obtain robotic walking in simulation utilizing only human data; the end result is surprisingly human-like robotic walking. This is quantified by comparing the outputs of AMBER to the human output data, and showing that it lies within one standard deviation of the norm, thus implying "normal" human walking [34]. To further validate the theory developed in this paper, we discuss the experimental implementation of the results presented on both AMBER and NAO. In both cases, we experimentally obtain human-inspired robotic walking on the physical robots (videos can be found at [2], [4]). This paper, therefore, formally and provably obtains robotic walking from human data, and realizes these formal results experimentally on two real-world bipedal robots.

This paper has drawn inspiration from work on robotic walking that attempts to discover the fundamental principles underlying bipedal walking, including but not limited to: passive walking and controlled symmetries [29], [14], [44], geometric reduction [8], [20], [41] and hybrid nonlinear feedback control [19], [51]. It is also important to note that this is not the first paper that attempts to bridge the gap between human and robotic walking [28], [40], [45], [46], although there have been relatively few studies in this direction when compared to the vast literature on robotic walking and biomechanics (see [11], [12], [13], [51] and [22], [49], [52], [32], to only name a few). Of special note is the preexisting work that studies human data in the context of both robotic walking and optimization [45], [46], [53]; a common thread in that work is that the human data considered consists of simply the joint angles over time, and this data is fit with high order polynomials. The results in this paper, therefore, substantially diverges from this preexiting work in two important and fundamental ways: (a) human output data is considered, rather than just angles, yielding a low-dimensional representation of human walking, and (b) this output data is described with canonical walking functions, giving insight into the behavior of these outputs over time that is of the simplest, yet most general, form possible. The hope is that by looking at outputs of the human described by canonical walking functions, the fundamental mechanisms underlying human walking can be discovered and exploited to achieve truly human-like bipedal robotic walking that, as a byproduct of this understanding, has the potential to be inherently robust.

It is important to note that the results presented in this paper build upon [5], [6], [7]. These papers considered human-inspired control of 4 and 5 link (under and fully) actuated robots in the context of specific output combinations. This paper generalizes and extends these constructions and results in the following significant ways: considers the hybrid system model of a general robot for which the previous models and the specific robots considered in this paper are a special case, introduces the general notion of a human output combination allowing for the freedom to choose different human outputs as long as they satisfy certain conditions, extends the formal results from [5], [6], [7] to this general setting, and introduces novel results related to the characterization of solutions and limit cycles in the context of full actuation—results that are essential to experimental realization. The main motivation for these generalizations are the recent results that build upon the human-inspired control framework. These include: walking up stairs, down stairs and running in simulation through the human-inspired control framework [37], [56], walking up slopes and on uneven terrain experimentally on AMBER 1 [33], walking flat ground (both in simulation and experimentally) for a fully actuated 2D robot with feet AMBER 2.0 [3], [54], and 3D speed regulated robotic walking with NAO both in simulation and experimentally [36]. At the core of all of these results are the formal results presented in this paper, thus indicating the extensibility of the formal results presented.

II. Bipedal Robot Models

Bipedal walking robots naturally display continuous and discrete behavior throughout the course of a step—the continuous behavior occurs when the leg swings forward and the discrete behavior occurs when the foot strikes the ground. It is, therefore, natural to model robots of this form by hybrid systems. This section introduces the basic formalisms of hybrid systems along with the specific hybrid models modeling bipedal robots. A special case of these systems yields the models for the two robots considered in this paper: AMBER and NAO (see Fig. 1 for pictures of both of these robots). Specifically, we consider two hybrid models, one for full actuation and one for underactuation.

Hybrid Systems. We begin by introducing hybrid (control) systems (also referred to as systems with impulsive effects or systems with impulse effects [19], [20]). We consider hybrid systems with one domain because the specific biped models considered in this paper do not have feet; the same model applies to robots with flat foot walking, while for more complex foot behavior more elaborate hybrid systems must be considered [20], [47], [41].

A (simple) *hybrid control system* is a tuple,

$$\mathscr{HC} = (\mathcal{D}, U, S, \Delta, f, g),$$

where $\mathcal{D}$ is the *domain* with $\mathcal{D} \subseteq R^n$ a smooth submanifold of the state space $\mathbb{R}^n$, $U \subseteq \mathbb{R}^m$ is the set of admissible controls, $S \subset \mathcal{D}$ is a proper subset of $\mathcal{D}$ called the *guard* or *switching surface*, $\Delta : S \to \mathcal{D}$ is a smooth map called the *reset map*, and (f, g) is a *control system* on $\mathcal{D}$, i.e., in coordinates: $\dot{x} = f(x) + g(x)u$. A *hybrid system* is a hybrid control system with $U = \emptyset$, e.g., any applicable feedback controllers have been applied, making the system closed-loop. In this case,

$$\mathscr{H} = (\mathcal{D}, S, \Delta, f),$$

where f is a *dynamical system* on $\mathcal{D} \subseteq \mathbb{R}^n$, i.e., $\dot{x} = f(x)$.

Periodic Orbits. Stable bipedal robotic walking corresponds to stable periodic orbits in hybrid systems. For simplicity, we focus our attention on introducing periodic orbits of hybrid systems with fixed

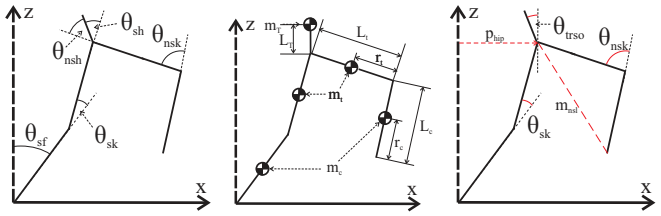

(a) Configuration (b) Mass/length (c) Constraints

Fig. 2: The modeled robot's configuration, mass & length distribution, and virtual constraints (outputs).

points on the guard (for more general definitions, see [20], [50]). Let $\varphi(t, x_0)$ be the solution to $\dot{x} = f(x)$ with initial condition $x_0 \in \mathcal{D}$. For $x* \in S$, we say that φ is *periodic* with period $T > 0$ if $\varphi(T, \Delta(x*)) = x*$. A set $\mathscr{O}$ is a *periodic orbit* with *fixed point* x^* if $\mathscr{O} = \{\varphi(t, x^*) : 0 \leq t \leq T\}$ for a periodic solution φ. Associated with a periodic orbit is a Poincaré map [50]. In particular, taking S to be the Poincaré section, one obtains the Poincaré map $P : S \to S$ which is a partial function:

$$P(x) = \varphi(T_I(x), \Delta(x)),$$

where $T_I : S \to \mathbb{R}_{>0}$ is the *time-to-impact function* [51]:

$$T_I(x) = \min\{t \geq 0 : \varphi(t, \Delta(x)) \in S\}, \tag{1}$$

for $x \in S$. As with smooth dynamical systems, the stability of the Poincaré map determines the stability of the periodic orbit $\mathscr{O}$. In particular, the Poincaré map is (locally) exponentially stable (as a discrete time system $x_{k+1} = P(x_k)$) at the fixed point x^* if and only if the periodic orbit $\mathscr{O}$ is (locally) exponentially stable [30]. Although it is typically not possible to analytically compute the Poincaré map, it is possible to numerically compute its Jacobian. If the eigenvalues of the Jacobian have magnitude less than 1, the stability of the periodic orbit $\mathscr{O}$ has been numerically verified.

Robotic Hybrid Models. Utilizing the formulation of hybrid systems, the remainder of this section is devoted to constructing hybrid system models for bipedal robots. Specifically, we consider two hybrid control systems corresponding to full and under actuation:

$$\mathscr{HC}_{R,\mathrm{FA}} = (\mathcal{D}_R, U_{R,\mathrm{FA}}, S_R, \Delta_R, f_R, g_{R,\mathrm{FA}}). \tag{2}$$

$$\mathscr{HC}_{R,\mathrm{UA}} = (\mathcal{D}_R, U_{R,\mathrm{UA}}, S_R, \Delta_R, f_R, g_{R,\mathrm{UA}}). \tag{3}$$

The constructions of these systems will be presented in general case of a robot with a single discrete phase of walking and, in the case of underactuation, we will assume 1 degree of underactuation. As a result they are applicable to both 2D and 3D robots in the case of full actuation. In the case of underactuation, due to the assumption on 1 degree of underactuation, they are only applicable to 2D underactuated robots or 3D robots with feet where the underactuation is, for example, a result of ankles with only one degree of actuation. In the case of 3D robots with point feet, more elaborate constructions are needed to understand the zero dynamics [21] due to the fact that they have higher dimensionality.

Note that the specific robot models for AMBER and NAO considered in this paper are just a special case of (2) and (3), with the type of actuation and parameters, e.g., masses, lengths and inertias, determined by the specific robot. For example, the mass and inertia properties for AMBER were obtained via a SolidWorks model and these constants were obtained for NAO through the published values at [1]. We suppress the dependence of the models on these parameters for notational simplicity.

Continuous Dynamics: Let $\mathcal{Q}_R$ be the configuration space of a robot with n degrees of freedom, i.e., $n = \dim(\mathcal{Q}_R)$, with coordinates $q \in \mathcal{Q}_R$. For the sake of definiteness, it may be necessary to choose $\mathcal{Q}_R$ to be a subset of the actual configuration space of the robot so that global coordinates can be defined[1], i.e., such that $\mathcal{Q}_R$ is embeddable in $\mathbb{R}^n$, or more simply $\mathcal{Q}_R \subset \mathbb{R}^n$. Calculating the mass and inertia properties of each link of the robot using the specifications of the robot allows for the construction of the Lagrangian $\mathcal{L}_R : T\mathcal{Q}_R \to \mathbb{R}$ of the form:

$$\mathcal{L}_R(\theta, \dot{\theta}) = \frac{1}{2}\dot{\theta}^T D(\theta)\dot{\theta} - V(\theta). \tag{4}$$

Explicitly, this is done symbolically through the method of twists and exponential maps (see [31]). The Euler-Lagrange equations yield the equations of motion of the form:

$$D(\theta)\ddot{q} + C(\theta, \dot{\theta}) = B_i(\theta)u. \tag{5}$$

where $i \in \{\mathrm{FA}, \mathrm{UA}\}$, i.e., B_i depends on the degree of actuation. In the case of full actuation $B_{\mathrm{FA}}(\theta) \in \mathbb{R}^{n\times n}$. In the case of underactuation, we will asumme one degree of underactuation, and therefore $B_{\mathrm{UA}}(\theta) \in \mathbb{R}^{n\times n-1}$.

Converting the equations of motion (5) to a first order ODE yields the affine control systems $(f_R, g_{R,i})$:

$$f_R(\theta, \dot{\theta}) = \begin{bmatrix} \dot{\theta} \\ -D^{-1}(\theta)C(\theta, \dot{\theta}) \end{bmatrix}, \quad g_{R,i}(\theta) = \begin{bmatrix} \mathbf{0} \\ D^{-1}(\theta)B_i(\theta) \end{bmatrix}.$$

where $i \in \{\mathrm{FA}, \mathrm{UA}\}$, i.e., we obtain control systems for both full and under actuation. Finally, the set of admissible values for control depends on the degree of actuation and the admissible control values, i.e, $U_{R,\mathrm{FA}} \subseteq \mathbb{R}^n$ and $U_{R,\mathrm{UA}} \subseteq \mathbb{R}^{n-1}$.

In the specific case of the robots AMBER and NAO, we will consider a 2D 5-link point foot model of both of these robots. In the case of AMBER this is a valid model of the system, since the robot is 2D operating on a boom while in the case of NAO this is a simplified model which only considers the sagittal dynamics and abstracts away the behavior of the feet which are compensated experimentally through local controllers. As a result of this choice of model, there are 5 degrees of freedom and the coordinates of $\mathcal{Q}_R$ are denoted by $\theta = (\theta_{sf}, \theta_{sk}, \theta_{sh}, \theta_{nsh}, \theta_{nsk})^T$ where, as illustrated in Fig. 2, θ_{sf} is the angle of the stance foot, θ_{sk} is the angle of the stance knee, θ_{sh} is the angle of the torso with the stance thigh, θ_{nsh} is the angle of the non-stance thigh with the torso, and θ_{nsk} is the angle of the non-stance (or swing) knee. Since NAO is fully actuated, based upon this choice of coordinates $B_{\mathrm{FA}}(\theta) = I_5$. Since AMBER is underactuated at the stance ankle, B_{UA} consists of the 2nd through 5th column of B_{FA}. For NAO and AMBER $U_{R,\mathrm{FA}} = \mathbb{R}^5$ and $U_{R,\mathrm{UA}} = \mathbb{R}^4$ respectively (since we will, for the sake of simplicity, not put any restrictions on the values of the controllers).

Domain and Guard: The domain specifies the allowable configuration of the system as specified by a unilateral constraint function h_R; for the biped considered in this paper, this function specifies that the non-stance foot must be above the ground, i.e., h_R is the height of the non-stance foot. In particular, the domain $\mathcal{D}_R$ is given by:

$$\mathcal{D}_R = \left\{(\theta, \dot{\theta}) \in T\mathcal{Q}_R : h_R(\theta) \geq 0\right\}.$$

The guard is just the boundary of the domain with the additional assumption that the unilateral constraint is decreasing:

$$S_R = \left\{(\theta, \dot{\theta}) \in T\mathcal{Q}_R : h_R(\theta) = 0 \text{ and } dh_R(\theta)\dot{\theta} < 0\right\},$$

where $dh_R(\theta)$ is the Jacobian of h_R at θ.

[1]Note that are various points we will assume that matrix functions have full rank; it may be necessary to carefully choose $\mathcal{Q}_R$ to satisfy these conditions.

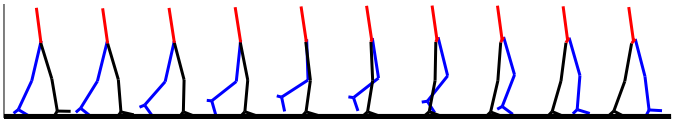

Fig. 3: Tiles of the walking gait for a human subject, plotted directly from the human walking data.

Discrete Dynamics. The discrete dynamics of the robot determine how the velocities of the robot change when the foot impacts the ground, while simultaneously switching the "stance" and "non-stance" legs. In particular, the reset map Δ_R is given by:

$$\Delta_R : S_R \to \mathcal{D}_R, \qquad \Delta_R(\theta, \dot{\theta}) = \begin{bmatrix} \Delta_\theta \theta \\ \Delta_{\dot{\theta}}(\theta)\dot{\theta} \end{bmatrix}, \tag{6}$$

where Δ_θ is the relabeling which switches the stance and non-stance leg at impact (by appropriately changing the angles). Here, $\Delta_{\dot{\theta}}$ determines the change in velocity due to impact; a detailed discussion on its computation can be found in [24], [20] and [5]. In particular, it is computed by considering extended coordinates that include the position of the stance foot and employing a perfectly plastic impact law that results in the pre-impact non-stance foot being fixed post-impact wherein it becomes the stance foot.

III. Human Output Combinations

Because the ultimate goal of this work is to develop a control scheme which yields stable human-like robotic walking, we begin by looking at human locomotion for motivation. In particular, we consider experimental human walking data, and from this data we seek a low-dimensional representation of human walking through *human outputs* and *canonical walking functions.* In particular, examination of human walking data reveals that certain outputs of the human locomotion system, i.e., functions of the kinematics which we term *human output functions*, can be represented as second order system responses. In other words, we find that certain outputs of the human are described by the time solution to a linear mass-spring-damper system:

$$y(t) = e^{-\zeta\omega_n t}(c_0 \cos(\omega_d t) + c_1 \sin(\omega_d t)) + g \tag{7}$$

where ζ is the damping ratio, ω_n is the natural frequency, $\omega_d = \omega_n\sqrt{1-\zeta^2}$ is the damped natural frequency, c_0 and c_1 are determined by the initial conditions of the system, and g is a "gravity" related constant. This section will provide evidence of this fact by considering human walking data and showing that functions of this form indeed describe human walking with exceptionally high correlation.

Human Walking Data. An integral part of the human-inspired nature of the control scheme presented is its motivation from human locomotion. This takes the form of data associated with human walking which will be considered throughout this paper. This data was collected from 9 subjects: 2 females and 7 males with ages ranging from 17 to 30, heights ranging from 160.0 cm to 188.5 cm, and weights ranging from 47.7 kg to 90.9 kg. The subjects walked 3 meters along a line drawn on the floor at a "natural" pace, with each subject performing 11 trials. For each trial, LED's were fixed to a test subject in key locations, such as the joints, along the lower body—as the test subject walked forward, the spatial position of each LED sensors was measured at 480 Hz. Details on the experiment and data analysis can be found in [5], [9].

For purposes of this paper, the mean data from all 9 subjects are considered. A single step, consisting of heel strike to heel strike is isolated (see Fig. 3). The end result is discrete times, $t^H[k]$, and discrete values for the angles of the human mapped to the 5-link robot model considered in this paper (see Fig. 2(a)), denoted by $\theta^H[k]$, where here $k \in \{1, \dots, K\} \subset \mathbb{N}$ with K the number of data points.

Human Outputs. We now construct a low-dimensional representation of human walking from the given experimental data through the use of human outputs. The goal is to determine a collection of output functions, one for each degree of freedom of the robot, that are independent (the decoupling matrix associated with these outputs must be non-singular) while simultaneously giving intuitive insight into human walking.

Definition 1: A *human output combination* is a tuple $Y^H = (\mathcal{Q}_R, y_1^H, y_2^H)$ consisting of a configuration space $\mathcal{Q}_R$, a velocity-modulating output $y_1^H : \mathcal{Q}_R \to \mathbb{R}$ and position-modulating outputs $y_2^H : \mathcal{Q}_R \to \mathbb{R}^{n-1}$. Let O be an indexing for y_2^H whereby $y_2^H(\theta) = \left[y_2^H(\theta)_i\right]_{i\in O}$. A set of human outputs are *independent* if[2],

$$\operatorname{rank}\left(\begin{bmatrix} y_1^H(\theta) \\ y_2^H(\theta) \end{bmatrix}\right) = n \tag{8}$$

on $\mathcal{Q}_R$, and *linear* if

$$y_1^H(\theta) = c\theta \tag{9}$$
$$y_2^H(\theta) = H\theta \tag{10}$$

for $c \in \mathbb{R}^{1\times n}$ and $H \in \mathbb{R}^{n-1\times n}$.

In the case of the robotic models considered in this paper, we will utilize the following human outputs:

$$y_1^H(\theta) = \delta p_{\text{hip}}(\theta) \tag{11}$$
$$y_2^H(\theta) = \begin{bmatrix} \delta m_{nsl}(\theta) \\ \theta_{sk} \\ \theta_{nsk} \\ \theta_{tor}(\theta) \end{bmatrix} \tag{12}$$

where

$$\delta p_{\text{hip}}(\theta) = L_c(-\theta_{sf}) + L_t(-\theta_{sf} - \theta_{sk}) \tag{13}$$
$$\delta m_{nsl}(\theta) = -\theta_{sf} - \theta_{sk} - \theta_{sh} + \theta_{nsh} + \frac{L_c}{L_c + L_t}\theta_{nsk} \tag{14}$$
$$\theta_{tor}(\theta) = \theta_{sf} + \theta_{sk} + \theta_{sh} \tag{15}$$

with δp_{hip} the linearization of the x-position of the hip, δm_{nsl} is the linearization of the slope of the non-stance leg m_{nsl}, (the tangent of the angle between the z-axis and the line on the non-stance leg connecting the ankle and hip), and θ_{tor} is the angle of the torso from zero. It is clear that this choice of human outputs are linear and independent. Denote the indexing set for the position-modulating outputs by $O = \{nsl, sk, nsk, tor\}$.

The human outputs $y_1^H(\theta^H[k])$ and $y_2^H(\theta^H[k])$ from (11) and (12) are computed from the experimental human walking data, $\theta^H[k]$, with the results given in Fig. 4. In addition, the error bands in the figure show one standard deviation from this mean human data. The simple form that the outputs take in Fig. 4 motivates the consideration of a special class of time based functions representing these outputs: canonical walking functions.

It is important to note that numerous other human outputs are possible, even in the case of the 5-link robot model considered in this paper. In particular, the actual position of the hip and non-stance slope, as nonlinear functions, were considered in [5], [43] yielding almost identical results. More generally, [43], [42] considers collections of human outputs and analyzes their ability to correctly describe human locomotion: examples of other velocity-modulating

[2]Here the rank is defined to be the rank of the Jacobian.

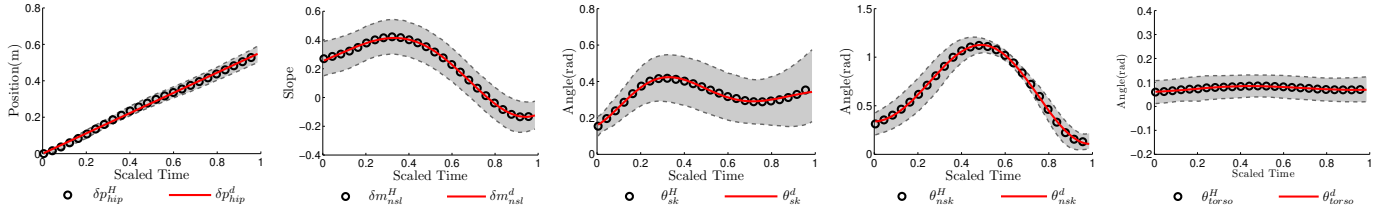

(a) δp_{hip} (b) δm_{nsl} (c) θ_{sk} (d) θ_{nsk} (e) θ_{tor}

Fig. 4: The mean human output data computed over one step (heel strike to heel strike) from the data of nine subjects walking, with error bands showing one standard deviation from the mean, and the canonical walking function fits (red). The data for the δp_{hip} was shifted to be zero at time zero.

outputs include the position of the center of mass, and position-modulating outputs such as the hip angle and leg lengths.

Canonical Walking Functions. Visually inspecting the human outputs, computed from the human data and shown in Fig. 4, they all appear to be described by two simple functions. In particular, the linearized position of the hip appears to be essentially a linear function of time:

$$y_1^H(\theta^H[k]) \approx v_{hip} t^H[k], \tag{16}$$

The remaining human outputs, δm_{nsl}, θ_{sk}, θ_{nsk}, θ_{tor} appear to be described by the solution to a linear mass-spring-damper system. With this in mind, define the *canonical walking function*:

$$y_H(t,\alpha) = e^{-\alpha_4 t}(\alpha_1 \cos(\alpha_2 t) + \alpha_3 \sin(\alpha_2 t)) + \alpha_5 \tag{17}$$

This function can be related to the more standard form of the time solution of a mass-spring-damper system given in (7) by noting that $\alpha_1 = c_0$, $\alpha_2 = \omega_d$, $\alpha_3 = c_1$, $\alpha_4 = \zeta\omega_n$ and $\alpha_5 = g$. In particular, with (17), for the 4 remaining human outputs, y_2^H, the claim is that we can desired their behavior as:

$$y_2^H(\theta^H[k]) \approx [y_H(t^H[k], \alpha_i)]_{i\in O} \tag{18}$$

where $\alpha_i = (\alpha_{i,1}, \alpha_{i,2}, \alpha_{i,3}, \alpha_{i,4}, \alpha_{i,5})$ in (17), and the parameters of all of the outputs can be combined to yield a single vector: $\alpha = (v_{\text{hip}}, \alpha_{nsl}, \alpha_{nsk}, \alpha_{sk}, \alpha_{tor}) \in \mathbb{R}^{21}$. If it can be verified that these functions accurately fit the mean human output data, then it can be concluded that humans appear to act like linear spring-mass-damper systems for the chosen outputs.

Human-Data-Based Cost Function. We now show that the canonical walking functions accurately describe the human data. This is achieved by simply fitting (17) to the human walking data to achieve a least-squares fit. While this can be done automatically with a wide variety of preexisting software, we prefer to achieve these fits by stating them in the form of an optimization problem. This is necessitated by two facts: (i) this same cost function will later be used to achieve robotic walking through a more sophisticated optimization problem, i.e., an optimization problem with constraints that formally guarantee stable robotic walking and (ii) it will form the basis for the notion of admissible output combinations.

Given a set of human outputs $Y^H = (\mathcal{Q}_R, y_1^H, y_2^H)$ as given in Definition 1 with associated human data $\theta^H[k] \in \mathcal{Q}_R$ defined at discrete times $t^H[k]$ with $k \in \{1, \dots, K\}$, define the following human-data-based cost function:

$$\begin{aligned}\text{Cost}_{\text{HD}}(\alpha) = &\sum_{k=1}^{K} (y_1^H(\theta^H[k]) - v t^H[k] - y_1^H(\theta^H[0]))^2 \\ &+ \sum_{i\in O} (y_2^H(\theta^H[k]) - y_H(t^H[k], \alpha_i))^2\end{aligned} \tag{19}$$

which is simply the sum of squared residuals, where here v represents a constant desired velocity (as will be seen in (21)) and $\alpha = (v, (\alpha_i)_{i\in O}) \in \mathbb{R}^{5n-4}$. To determine the parameters for the human walking functions, we need only solve the optimization problem:

$$\alpha^* = \underset{\alpha\in\mathbb{R}^{5n-4}}{\text{argmin}} \ \text{Cost}_{\text{HD}}(\alpha) \tag{20}$$

which yields the least squares fit of the mean human output data with the canonical walking functions. Therefore, given a set of human outputs, these outputs are accurately described by the canonical walking function if $\text{Cost}_{\text{HD}}(\alpha^*)$ is "small." This, coupled with the desire to utilize the human outputs in controller design, motivates the following definition of admissible human output combinations.

Definition 2: For $\delta > 0$ sufficiently small, The human output combination $Y^H = (\mathcal{Q}_R, y_1^H, y_2^H)$ is *admissible* if the decoupling matrix $\mathcal{A}_{\text{FA}}$ given in (29) is nonsingular and δ-*admissible* if the parameters solving (20) satisfy $\text{Cost}_{\text{HD}}(\alpha^*) < \delta$.

The main idea behind admissible human output combinations is that one should choose output combinations that are accurately described by the canonical walking function. Doing so will facilitate the human-inspired control introduced in Section IV; this is where the admissibility of the outputs will be formalized through the introduction of the decoupling matrix. The requirement that $\text{Cost}_{\text{HD}}(\alpha^*) < \delta$ stems from the fact that because human data can vary, a perfect fit is never possible but it should be "good enough." The size, δ, of this variation between the time based representation and the actual data should be kept small; naturally, this is both a function of the data collection and the choice of outputs. In addition, since the human-inspired optimization introduced in Section V will minimize (19) subject to constraints, having a small initial value of the cost is desirable.

In the case of AMBER and NAO, the same human output combinations, (11) and (12), are considered; it is easy to verify that this output combination is admissible. Solving the optimization problem (20) results in the parameters stated in Table I. In this case $\text{Cost}_{\text{HD}}(\alpha^*) = 0.0447$, and therefore, this output combination is δ-admissible with, for example, $\delta = 0.05$. The small value of δ indicates that the canonical walking function accurately describes the human data for the outputs chosen; this is further supported by the coefficients of correlation given in Table I which range between 0.9862 to 0.999 and visually through Fig. 4; note that the correlations for detrended and zero mean data are essentially the same. This provides evidence that the canonical walking function appears to, in fact, be canonical in some sense due to the small number of parameters needed to accurately describe the human data coupled with the intuitive representation of human walking given—humans appear to act like linear spring-mass-damper systems with respect to certain outputs.

It is important to note that the human outputs considered, and the fact that humans act like linear mass-spring-dampers for these outputs, provides evidence for many of the "human-inspired" constructions considered in the past. In particular, the specific choice of human outputs was motivated by the compass gait biped [8], [16], [17], [43]; in essence, the (nonlinear) form of these outputs represent the human as a compass gait biped. Moreover, the specific choice of canonical function is motivated by the well-studied SLIP model [35], [27], [23] in that it represents human walking as essentially being the behavior of a linear mass-spring-damper system for the outputs chosen. Finally, it is important to note that the viewpoint on human walking taken in this paper, and the fact that output functions of a very special form are considered, differentiates it from other work that has considered human data because previous work considers, almost exclusively, joint angles over time [45], [46], [53]

IV. Human-Inspired Control

In this section, we construct a *human-inspired controller* that drives the outputs of the robot to the outputs of the human (as represented by canonical walking functions). In particular, in both the case of full and under actuation, we consider an admissible output combination $Y^H = (\mathcal{Q}_R, y_1^H, y_2^H)$ and construct a feedback controller through the use of a parametrization of time based upon the velocity-modulating output. The end result are feedback controllers that will be used to obtain stable bipedal robotic walking.

Output Functions. Based upon the human outputs and their time-based representation given by the canonical walking functions, we define outputs for the robot based upon our desire for the robot to have the same output behavior as the human. With the goal of controlling the velocity of the robot, we define the relative degree 1 outputs to be the velocity of the velocity-modulating output—hence the motivation for the name—and a desired velocity:

$$y_{a,1}(\theta,\dot\theta) = \dot y_1^H(\theta,\dot\theta) = dy_1^H(\theta)\dot\theta, \qquad y_{d,1}(\alpha) = v. \tag{21}$$

Similarly, with the goal of the robot tracking the canonical walking function (18) through the position-modulating outputs, we consider the following actual and desired outputs:

$$y_{a,2}(\theta) = y_2^H(\theta), \qquad y_{d,2}(t,\alpha) = \left[\ y_H(t,\alpha_i)\ \right]_{i\in O}. \tag{22}$$

In the case when $Y^H = (\mathcal{Q}_R, y_1^H, y_2^H)$ is a linear and independent output combination, it follows that:

$$\begin{array}{rcll} y_{a,1}(\theta,\dot\theta) & = & c\dot\theta & \\ y_{a,2}(\theta) & = & H\theta & \text{s.t.} \quad \operatorname{rank}\left(\begin{bmatrix} c \\ H \end{bmatrix}\right) = n, \end{array} \tag{23}$$

by (8)-(10).

Parameterization of Time. Motivated by the desire to create an *autonomous* controller, which are more robust than time based controllers, we introduce a state-based parameterization of time in our system as is common practice [45], [51]. Examination of human data reveals that the (linearized) forward position of the hip evolves in an approximately linear manner with respect to time (16). Taking advantage of this observation, for an admissible output combination $Y^H = (\mathcal{Q}_R, y_1^H, y_2^H)$, the following parameterization of time is considered:

$$\tau(\theta) = \frac{y_1^H(\theta) - y_1^H(\theta^+)}{v}. \tag{24}$$

where $y_1^H(\theta^+)$ is the value of the velocity-modulating output of the robot's hip at the beginning of the current step, and v is, as will be seen, the desired velocity (which is just an element of the vector of parameters $\alpha \in \mathbb{R}^{5n-4}$).

Fully Actuated Control. The goal is to drive the outputs of the robot, obtained through a human output combination, to the outputs of the human as represented by the canonical walking functions parameterized by $\tau(\theta)$. This motivates the final form of the outputs, termed the *human-inspired outputs* for full actuation, given by:

$$y_1(\theta,\dot\theta) = y_{a,1}(\theta,\dot\theta) - v, \tag{25}$$

$$y_2(\theta) = y_{a,2}(\theta) - y_{d,2}(\tau(\theta),\alpha). \tag{26}$$

These outputs can be grouped together to form a single vector of outputs:

$$y(\theta,\dot\theta) = \begin{bmatrix} y_1(\theta,\dot\theta) \\ y_2(\theta) \end{bmatrix} \tag{27}$$

where y_1 and y_2 will be seen to be relative degree 1 and (vector) relative degree 2 outputs, respectively, due to the assumption of admissible output combinations coupled with the fact that y_2 is the output to a mechanical system that is only dependent on θ.

The feedback linearization controller for full actuation, denoted by $u_{\text{FA}}^{(\alpha,\varepsilon)}(\theta,\dot\theta)$ and termed the *human-inspired controller* for full actuation due to its dependence on the human-inspired outputs, can now be stated as:

$$\begin{aligned} u_{\text{FA}}^{(\alpha,\varepsilon)}(\theta,\dot\theta) = -\mathcal{A}_{\text{FA}}^{-1}(\theta,\dot\theta)\Bigg(&\begin{bmatrix} 0 \\ L_{f_R}L_{f_R}y_2(\theta) \end{bmatrix} \\ &+ \begin{bmatrix} L_{f_R}y_1(\theta,\dot\theta) \\ 2\varepsilon L_{f_R}y_2(\theta,\dot\theta) \end{bmatrix} + \begin{bmatrix} \varepsilon y_1(\theta,\dot\theta) \\ \varepsilon^2 y_2(\theta) \end{bmatrix}\Bigg), \end{aligned} \tag{28}$$

with control gain ε and decoupling matrix:

$$\mathcal{A}_{\text{FA}}(\theta,\dot\theta) = \begin{bmatrix} L_{g_{R,\text{FA}}}y_1(\theta,\dot\theta) \\ L_{g_{R,\text{FA}}}L_{f_R}y_2(\theta,\dot\theta) \end{bmatrix}. \tag{29}$$

Note that the decoupling matrix is non-singular by the definition of an admissible output combination (see Def. 2). More generally, this follows from the fact that care was taken when defining the human output combinations so that they are independent (see Def. 1). It follows that $u_{\text{FA}}^{(\alpha,\varepsilon)}(\theta,\dot\theta)$ results in dynamics on the outputs given by:

$$\dot y_1 = -\varepsilon y_1 \tag{30}$$

$$\ddot y_2 = -2\varepsilon\dot y_2 - \varepsilon^2 y_2 \tag{31}$$

and therefore, for a control gain $\varepsilon > 0$, the control law $u_{\text{FA}}^{(\alpha,\varepsilon)}$ renders the output exponentially stable [39]. That is, the human-inspired outputs $y_1 \to 0$ and $y_2 \to 0$ exponentially at a rate of ε; in other words, the outputs of the robot will converge to the canonical walking functions exponentially.

Applying the feedback control law in (28) to the hybrid control system modeling the bipedal robot being considered, $\mathscr{HC}_{R,\text{FA}}$ as given in (2), yields a hybrid system:

$$\mathscr{H}_{R,\text{FA}}^{(\alpha,\varepsilon)} = (\mathcal{D}_R, S_R, \Delta_R, f_{R,\text{FA}}^{(\alpha,\varepsilon)}), \tag{32}$$

where, $\mathcal{D}_R$, S_R, and Δ_R are defined as for $\mathscr{HC}_{R,\text{FA}}$, and

$$f_{R,\text{FA}}^{(\alpha,\varepsilon)}(\theta,\dot\theta) = f_R(\theta,\dot\theta) + g_{R,\text{FA}}(\theta,\dot\theta)u_{\text{FA}}^{(\alpha,\varepsilon)}(\theta,\dot\theta), \tag{33}$$

$y_H = e^{-\alpha_4 t}(\alpha_1\cos(\alpha_2 t) + \alpha_3\sin(\alpha_2 t)) + \alpha_5$							
Fun.	v	α_1	α_2	α_3	α_4	α_5	Cor.
δp_{hip}	0.9337	*	*	*	*	*	0.9991
δm_{nsl}	*	0.0117	8.6591	0.1153	-2.1554	0.2419	0.9997
θ_{sk}	*	-0.1739	13.6644	0.0397	3.3222	0.3332	0.9934
θ_{nsk}	*	-0.3439	10.5728	0.0464	-0.8606	0.6812	0.9996
θ_{tor}	*	-0.0166	10.4416	-0.0033	3.2976	0.0729	0.9862

TABLE I: The parameter values of the canonical walking functions obtained from fitting the mean human data, together with the correlations of the fits.

where the dependence of $f_{R,\mathrm{FA}}^{(\alpha,\varepsilon)}$ on the vector of parameters of the canonical walking functions, α, and the control gain for the input/output linearization control law, ε, has been made explicit.

Underactuated Control. When the robot is underactuated, there is no longer the control authority to drive all of the outputs of the system to be in agreement with the human outputs. In particular, since we will no longer have control of the stance ankle (as in the case of AMBER, due to its point feet), we can no longer directly control the forward movement of the hip through the output (25). Thus, in the case of underactuation, we only consider the relative degree 2 outputs given in (26).

Motivated by these considerations related to underactuated control, for the affine control system $(f_R, g_{R,\mathrm{UA}})$ associated with the robotic model (3), we define the *human-inspired controller* for underactuation:

$$u_{\mathrm{UA}}^{(\alpha,\varepsilon)}(\theta,\dot\theta) = \\ -\mathcal{A}_{\mathrm{UA}}^{-1}(\theta,\dot\theta)\left(L_{f_R}^2 y_2(\theta,\dot\theta) + 2\varepsilon L_{f_R} y_2(\theta,\dot\theta) + \varepsilon^2 y_2(\theta)\right), \tag{34}$$

with y_2 as defined in (26) and $\mathcal{A}_{\mathrm{UA}}$ the underactuated decoupling matrix: $\mathcal{A}_{\mathrm{UA}}(\theta,\dot\theta) = L_{g_{R,\mathrm{UA}}} L_{f_R} y_2(\theta,\dot\theta)$. As in the case of full actuation, the decoupling matrix is non-singular because of the choice of output functions and the fact that we assume admissibility of the outputs. In addition, the control law $u_{\mathrm{UA}}^{(\alpha,\varepsilon)}$ results in dynamics on the outputs given by (31) and therefore renders the relative degree two outputs, y_2, exponentially stable, i.e., $y_2 \to 0$ exponentially at a rate of ε. Due to the fact that the system is underactuated, the output y_1 will no longer converge to 0. Thus the velocity of the hip cannot be directly controlled in the case of underactuation.

Applying the feedback control law in (34) to the hybrid control system modeling and a bipedal robot with 1 degree of underactuation, $\mathscr{HC}_{R,\mathrm{UA}}$ as given in (3), yields a hybrid system:

$$\mathscr{H}_{R,\mathrm{UA}}^{(\alpha,\varepsilon)} = (\mathcal{D}_R, S_R, \Delta_R, f_{R,\mathrm{UA}}^{(\alpha,\varepsilon)}), \tag{35}$$

where, $\mathcal{D}_R$, S_R, and Δ_R are defined as for $\mathscr{HC}_{R,\mathrm{UA}}$, and

$$f_{R,\mathrm{UA}}^{(\alpha,\varepsilon)}(\theta,\dot\theta) = f_R(\theta,\dot\theta) + g_{R,\mathrm{UA}}(\theta,\dot\theta) u_{\mathrm{UA}}^{(\alpha,\varepsilon)}(\theta,\dot\theta).$$

V. Human-Inspired Partial Hybrid Zero Dynamics

This section considers the fully actuated model of a bipedal robot $\mathscr{H}_{R,\mathrm{FA}}^{(\alpha,\varepsilon)}$, with the goal of formally obtaining human-like bipedal robotic walking. In particular, we determine parameters of the human-inspired controller that result in the best fit with the human output data while simultaneously guaranteeing robotic walking. To this end, we introduce a novel concept termed *partial hybrid zero dynamics* (PHZD), and present an optimization problem that determines the parameters that provide the best fit to the human data while ensuring PHZD. In addition, we prove that these parameters—as a consequence of the satisfaction of the PHZD constraints—will automatically guarantee robotic walking. The fixed point of this walking gait is explicitly constructed, and it is formally proven that the periodic orbit associated with this fixed point is locally exponentially stable.

Throughout this section, and the remainder of this paper, we make the following assumption:

A1: *The human output combination $Y^H = (\mathcal{Q}_R, y_1^H, y_2^H)$ is linear, independent and δ-admissible.*

Full Hybrid Zero Dynamics (FHZD). As stated in Section IV, the goal of the control law $u_{\mathrm{FA}}^{(\alpha,\varepsilon)}$ (28) is to drive the human-inspired output $y(\theta,\dot\theta) \to 0$ exponentially at a rate of ε. Therefore, for the *continuous* dynamics, the controller renders the *full zero dynamics surface*:

$$\mathbf{FZ}_\alpha = \{(\theta,\dot\theta) \in T\mathcal{Q}_R : y(\theta,\dot\theta) = \mathbf{0},\ L_{f_R} y_2(\theta,\dot\theta) = \mathbf{0}\} \tag{36}$$

exponentially stable; moreover, this surface is invariant for the continuous dynamics of the hybrid system $\mathscr{H}_{R,\mathrm{FA}}^{(\alpha,\varepsilon)}$. Note that here $\mathbf{0}$ is a vector of zeros of appropriate dimension and we make the dependence of $\mathbf{FZ}_\alpha$ on the set of parameters explicit. It is at this point that continuous systems and hybrid systems diverge: while this surface is invariant for the continuous dynamics, it is not necessarily invariant for the hybrid dynamics. In particular, the discrete impacts in the system cause the state to be "thrown" off of the full zero dynamics surface. Therefore, a hybrid system has *full hybrid zero dynamics (FHZD)* if the full zero dynamics are invariant through impact: $\Delta_R(S_R \cap \mathbf{FZ}_\alpha) \subset \mathbf{FZ}_\alpha$. It turns out that this condition is too strong in that—due to the differences between the robotic model and the human—it is not possible to obtain "good" walking that satisfies this requirement. Instead, due to these differences, it is more beneficial to allow the velocity of the hip to "jump" through impact, while requiring the other relative degree 2 outputs to remain on the invariant. This motivates the consideration of partial hybrid zero dynamics.

Partial Hybrid Zero Dynamics (PHZD). While the realization of FHZD is the "best case scenario," it is quite difficult in the case of bipedal robotic walking since it would force the hybrid system to evolve on a 1-dimensional manifold. Therefore, we enforce zero dynamics only for the relative degree 2 outputs. We refer to this as the *partial zero dynamics surface*, given by:

$$\mathbf{PZ}_\alpha = \{(\theta,\dot\theta) \in T\mathcal{Q}_R : y_2(\theta) = \mathbf{0},\ L_{f_R} y_2(\theta,\dot\theta) = \mathbf{0}\} \tag{37}$$

The motivation for considering this surface is that it allows some "freedom" in the movement of the system to account for differences between the robot and human models. Moreover, since the only output that is not included in the partial zero dynamics surface is the output that forces the forward hip velocity to be constant, enforcing partial hybrid zero dynamics simply means that we allow the velocity of the hip to compensate for the shocks in the system due to impact.

Problem Statement. The goal of *human-inspired PHZD* is to find parameters α^* that solve the following constrained optimization problem:

$$\alpha^* = \underset{\alpha\in\mathbb{R}^{5n-4}}{\operatorname{argmin}}\ \mathrm{Cost}_{\mathrm{HD}}(\alpha) \tag{38}$$
$$\text{s.t}\quad \Delta_R(S_R \cap \mathbf{PZ}_\alpha) \subset \mathbf{PZ}_\alpha \qquad \text{(PHZD)}$$

with $\mathrm{Cost}_{\mathrm{HD}}$ the cost given in (19). This is simply the optimization problem in (20) that was used to determine the parameters of the canonical walking functions that gave the best fit of the human walking functions to the human output data, but subject to constraints that ensure PHZD. The formal goal of this section is to restate (PHZD) in such a way that it can be solved practically.

Partial Zero Dynamics. This section utilizes the fact that the human outputs were specifically chosen to be linear in order to explicitly construct the *partial hybrid zero dynamics*. In particular, we reformulate the constructions in [51] in a way applicable to full-actuation and reframed in the context of canonical walking functions. Because of the specific form of $y_{a,1}$ in (23) due to the linear output assumption, we begin by picking the following coordinates for the partial zero dynamics surface:

$$\begin{aligned} z_1 &= y_1^H(\theta) = c\theta \\ z_2 &= y_{a,1}(\theta,\dot\theta) = \dot y_1^H(\theta,\dot\theta) = c\dot\theta \end{aligned} \tag{39}$$

where $c \in \mathbb{R}^{1\times n}$ is obtained from (9). Moreover, since z_1 is just the velocity-modulating output, which was used to parameterize time (24), we can write $y_{d,2}(z_1) = y_{d,2}(\tau(\theta),\alpha)$. Picking the coordinates

$$\begin{aligned} \eta_1 &= y_{a,2}(\theta) = H\theta \\ \eta_2 &= L_{f_R} y_{a,2}(\theta,\dot\theta) = H\dot\theta \end{aligned} \tag{40}$$

with H as in (10), and defining

$$\begin{aligned}\Phi_{\mathbf{PZ}}(z_1) &= \begin{bmatrix} c \\ H \end{bmatrix}^{-1} \begin{pmatrix} z_1 \\ y_{d,2}(z_1) \end{pmatrix} \\ \Psi_{\mathbf{PZ}}(z_1) &= \begin{bmatrix} c \\ H \end{bmatrix}^{-1} \begin{pmatrix} 1 \\ \frac{\partial y_{d,2}(z_1)}{\partial z_1} \end{pmatrix}\end{aligned} \tag{41}$$

it follows that for $\theta = \Phi_{\mathbf{PZ}}(z_1)$ and $\dot\theta = \Psi_{\mathbf{PZ}}(z_1)z_2$, the point $(\theta, \dot\theta) \in \mathbf{PZ}_\alpha$.

As a result of the fact that we have full actuation and completely linearize the dynamics with (28), it follows that the relative degree 1 output (25) evolves according to $\dot y_1 = -\varepsilon y_1$. Therefore, the partial hybrid zero dynamics evolve according to the linear ODE:

$$\begin{aligned}\dot z_1 &= z_2 \\ \dot z_2 &= -\varepsilon(z_2 - v).\end{aligned} \tag{42}$$

The advantage of the partial zero dynamics representation introduced is that its linear form allows for the existence and stability of a fixed point of the zero dynamics to be determined *in closed form*. Specifically, given a pre-impact point on the guard $(\theta^-, \dot\theta^-) \in S_R$ with its post-impact state $(\theta^+, \dot\theta^+) = \Delta_R(\theta^-, \dot\theta^-)$, we can compute $z_1^- = y_1^H(\theta^-)$ and $z_1^+ = y_1^H(\theta^+)$. From this, if (PHZD) is satisfied, the change in z_1 and z_2 due to this impact can be determined through:

$$\begin{aligned}z_1^+ &= y_1^H(\Delta_\theta \theta^-) \\ z_2^+ &= \Delta_{\mathbf{PZ}}(\theta^-) z_2^-\end{aligned} \tag{43}$$

where θ^- is a point that is chosen *a priori* and

$$\Delta_{\mathbf{PZ}}(\theta^-) := c\Delta_{\dot\theta}(\theta^-)\Psi_{\mathbf{PZ}}(y_1^H(\theta^-)) \tag{44}$$

In essence, this defines a 2-dimensional hybrid system and since the partial hybrid zero dynamics is 2-dimensional, when considering the existence and stability of a periodic orbit in this surface one need only consider the restricted Poincaré map:

$$\rho_\varepsilon : S_R \cap \mathbf{PZ}_\alpha \to S_R \cap \mathbf{PZ}_\alpha \tag{45}$$

where ρ_ε depends on ε due to (42) and

$$S_R \cap \mathbf{PZ}_\alpha \cong \{(z_1, z_2) \in \mathbf{PZ}_\alpha : \ z_1 = z_1^-, \quad z_2 \in \mathbb{R}_{\geq 0}\}. \tag{46}$$

In other words, the hyperplane $z_1 = z_1^-$ can be chosen as the Poincaré section. The Poincaré map for the partial hybrid zero dynamics is therefore a 1-dimensional (partial) map $\rho_\varepsilon : S_R \cap \mathbf{PZ}_\alpha \to S_R \cap \mathbf{PZ}_\alpha$, and so ρ can be viewed as only a function of z_2 which therefore defines a discrete time dynamical system:

$$z_2[k+1] = \rho_\varepsilon(z_2[k])$$

and the stability of this 1-dimensional discrete time dynamical system, as will be seen in Theorem 2, completely determines the stability of a periodic orbit in the full dimensional system.

Inverse Kinematics. To achieve the goal of restating (38) in a way that is independent of state variables (position and velocity), we seek to explicitly construct the point $(\theta^-, \dot\theta^-)$ that will be utilized in the constructions outlined in (43) and (44). To this end, we can use the outputs and guard functions to explicitly solve for the configuration of the system $\vartheta(\alpha) \in \mathcal{Q}_R$ on the guard $(h_R(\vartheta(\alpha)) = 0)$ in terms of the parameters α. In particular, let

$$\vartheta(\alpha) = \theta \quad \text{s.t} \quad \begin{bmatrix} y_2(\Delta_\theta \theta) \\ h_R(\theta) \end{bmatrix} = \begin{bmatrix} \mathbf{0} \\ 0 \end{bmatrix}, \tag{47}$$

where Δ_θ is the relabeling matrix (6). Note that $\vartheta(\alpha)$ exists because of the specific structure of the outputs, $y_2(\Delta_\theta\theta)$, chosen. In fact, the reason for considering y_2 at $\Delta_\theta\theta$ is because it implies that the configuration at the beginning of the step is $\theta^+ = \Delta_\theta\theta$ and thus $\tau(\Delta_\theta\theta) = 0$ implying that: $y_2(\Delta_\theta\theta) = H\Delta_\theta\theta - y_{d,2}(0, \alpha)$, or there is a solution to (47) because of the simple form that y_2 takes at $\Delta_\theta\theta$.

Using $\vartheta(\alpha)$, we can explicitly solve for a point $(\vartheta(\alpha), \dot\vartheta(\alpha)) \in \mathbf{FZ}_\alpha \cap S_R$. In particular, let

$$Y(\theta) = \begin{bmatrix} dy_1^H(\theta) \\ dy_2(\theta) \end{bmatrix}, \tag{48}$$

It follows from the definition of y_1 and y_2 in (25) and (26) that

$$\begin{bmatrix} y_1(\theta, \dot\theta) \\ L_{f_R} y_2(\theta, \dot\theta) \end{bmatrix} = Y(\theta)\dot\theta - \begin{bmatrix} v \\ \mathbf{0} \end{bmatrix}. \tag{49}$$

Therefore, define

$$\dot\vartheta(\alpha) = Y^{-1}(\vartheta(\alpha)) \begin{bmatrix} v \\ \mathbf{0} \end{bmatrix}, \tag{50}$$

where Y is invertible because of the choice of outputs. The point $(\vartheta(\alpha), \dot\vartheta(\alpha))$ is essential to all of the constructions in this paper, as it will: (a) be used to remove state-dependence in the optimization, (b) be a fixed point of a periodic orbit, and (c) will be used to determine the stability of the periodic orbit by taking it to be the point chosen *a priori* in (43).

Human-Inspired Optimization. With the notation of this section in hand, we define a *human-inspired optimization problem* (first introduced in [5]). This constrained optimization uses the human data as a cost function (through the human-data-based cost (19)), but enforces constraints that, as will be seen in the main result, ensure that the bipedal robot has a stable walking gait.

Theorem 1: *The parameters α^* solving the constrained optimization problem:*

$$\alpha^* = \underset{\alpha \in \mathbb{R}^{5n-4}}{\operatorname{argmin}} \ \operatorname{Cost}_{\mathrm{HD}}(\alpha) \tag{HIO}$$

$$\begin{aligned} \text{s.t} \quad & y_2(\vartheta(\alpha)) = \mathbf{0} && \text{(C1)} \\ & dy_2(\Delta_\theta \vartheta(\alpha))\Delta_{\dot\theta}(\vartheta(\alpha))\dot\vartheta(\alpha) = \mathbf{0} && \text{(C2)} \\ & dh_R(\vartheta(\alpha))\dot\vartheta(\alpha) < 0 && \text{(C3)} \end{aligned}$$

yield partial hybrid zero dynamics: $\Delta_R(S_R \cap \mathbf{PZ}_{\alpha^*}) \subset \mathbf{PZ}_{\alpha^*}$.

Proof: Let α^* be the solution to the optimization problem (HIO). We begin by showing that $\Delta_R(S_R \cap \mathbf{FZ}_{\alpha^*}) \subset \mathbf{PZ}_{\alpha^*}$ since this will imply that $\Delta_R(S_R \cap \mathbf{PZ}_{\alpha^*}) \subset \mathbf{PZ}_{\alpha^*}$. By (C1) and (49), $(\vartheta(\alpha^*), \dot\vartheta(\alpha^*)) \in \mathbf{FZ}_{\alpha^*}$. Moreover, by (47) (specifically, the fact that $h_R(\vartheta(\alpha^*)) = 0$) and (C3), it follows that $(\vartheta(\alpha^*), \dot\vartheta(\alpha^*)) \in S_R$. Therefore, $(\vartheta(\alpha^*), \dot\vartheta(\alpha^*)) \in S_R \cap \mathbf{FZ}_{\alpha^*}$. Now, $\mathbf{FZ}_{\alpha^*}$ and S_R intersect transversally since

$$L_{f_R} h_R(\vartheta(\alpha^*), \dot\vartheta(\alpha^*)) = dh_R(\vartheta(\alpha^*))\dot\vartheta(\alpha^*) < 0$$

by (C3). Since $\mathbf{FZ}_{\alpha^*}$ is a 1-dimensional submanifold of $\mathcal{D}_R$, it follows that $S_R \cap \mathbf{FZ}_{\alpha^*}$ is a unique point. Therefore, $(\vartheta(\alpha^*), \dot\vartheta(\alpha^*)) = S_R \cap \mathbf{FZ}_{\alpha^*}$.

To show that $\Delta_R(S_R \cap \mathbf{FZ}_{\alpha^*}) \subset \mathbf{PZ}_{\alpha^*}$ we need only show that $\Delta_R(\vartheta(\alpha^*), \dot\vartheta(\alpha^*)) \in \mathbf{PZ}_{\alpha^*}$. From the form of Δ_R given in (6), the requirement that $\Delta_R(\vartheta(\alpha^*), \dot\vartheta(\alpha^*)) \in \mathbf{PZ}_{\alpha^*}$ is equivalent to the following conditions being satisfied:

$$y_2(\Delta_\theta \vartheta(\alpha^*)) = 0, \tag{51}$$

$$L_{f_R} y_2(\Delta_\theta \vartheta(\alpha^*), \Delta_{\dot\theta}(\vartheta(\alpha^*))\dot\vartheta(\alpha^*)) = 0. \tag{52}$$

By the definition of $\vartheta(\alpha^*)$, and specifically (47), (51) is satisfied. Moreover,

$$\begin{aligned} L_{f_R} y_2(\Delta_\theta \vartheta(\alpha^*), &\Delta_{\dot\theta}(\vartheta(\alpha^*))\dot\vartheta(\alpha^*)) = \\ & dy_2(\Delta_\theta \vartheta(\alpha^*))\Delta_{\dot\theta}(\vartheta(\alpha^*))\dot\vartheta(\alpha^*) \end{aligned}$$

Therefore, (52) is satisfied as a result of (C2). Thus we have established that $\Delta_R(S_R \cap \mathbf{FZ}_{\alpha^*}) \subset \mathbf{PZ}_{\alpha^*}$.

To complete the proof we note that $\Delta_R(S_R \cap \mathbf{FZ}_{\alpha^*}) \subset \mathbf{PZ}_{\alpha^*}$ implies that $\Delta_R(S_R \cap \mathbf{PZ}_{\alpha^*}) \subset \mathbf{PZ}_{\alpha^*}$ by Theorem 5.2 in [51] since $(\vartheta(\alpha^*), \dot{\vartheta}(\alpha^*)) = S_R \cap \mathbf{FZ}_{\alpha^*} \subset S_R \cap \mathbf{PZ}_{\alpha^*}$ is a point satisfying (51) and (52). ∎

Exact Reconstruction. One of the main advantages to considering partial hybrid zero dynamics in the case of full actuation is the simple form that the partial zero dynamics takes. In particular, using (42) we can explicitly, and in closed form, reconstruct the solution of the full-order system. This is outlined in the following proposition—a result that is essential to both proving the main result in the case of full actuation along with adding constraints that ensure the physical realizability of the resulting walking gait.

Consider the point $(\vartheta(\alpha^*), \dot{\vartheta}(\alpha^*)) \in \mathbf{PZ}_{\alpha^*} \cap S_R$ and let $z_1^-(\alpha^*)$ and $z_2^-(\alpha^*)$ be the representation of this point in the partial hybrid zero dynamics coordinates (39); note that from (50), $z_2^-(\alpha^*) = v^*$. By picking $\theta^- = \vartheta(\alpha^*)$ in (43), we obtain $z_1^+(\alpha^*)$. From the constructions presented in this section, and because $\Delta_R(S_R \cap \mathbf{PZ}_{\alpha^*}) \subset \mathbf{PZ}_{\alpha^*}$, by viewing $S_R \cap \mathbf{PZ}_{\alpha^*}$ as a 1-dimensional space as in (46), for an initial condition $z_2 \in S_R \cap \mathbf{PZ}_{\alpha^*}$ it follows from (42) that the solution to the partial hybrid zero dynamics are given by:

$$\begin{aligned} z_1(t, \alpha^*) &:= tv^* + z_1^+(\alpha^*) \\ &\quad + \frac{(1 - e^{-t\varepsilon})\Delta_{\mathbf{PZ}}(\vartheta(\alpha^*))z_2 + (-1 + e^{-t\varepsilon})v^*}{\varepsilon} \\ z_2(t, \alpha^*) &:= v^* + e^{-t\varepsilon}(\Delta_{\mathbf{PZ}}(\vartheta(\alpha^*))z_2 - v^*) \end{aligned} \tag{53}$$

With this notation in hand, we present the following result on reconstructing solutions for the full order system in closed form through partial hybrid zero dynamics.

Proposition 1: *Let α^* be the parameters solving* (HIO) *and assume that*

$$\tau(\vartheta(\alpha^*)) = \frac{z_1^-(\alpha^*) - z_1^+(\alpha^*)}{v^*} > 0.$$

For $z_2 \in S_R \cap \mathbf{PZ}_{\alpha^*}$, the time-to-impact function for the partial hybrid zero dynamics is given by:

$$T_{\mathbf{PZ}}(z_2) = \tau(\vartheta(\alpha^*)) + \frac{1}{\varepsilon v^*}\left(-\Delta_{\mathbf{PZ}}(\vartheta(\alpha^*))z_2 + \rho_\varepsilon(z_2)\right)) \tag{54}$$

with

$$\rho_\varepsilon(z_2) = v^*\left(1 + \mathcal{W}(e^{-\varepsilon\tau(\vartheta(\alpha^*))}e^{\gamma(z_2)}\gamma(z_2)\right) \tag{55}$$

where $\mathcal{W}$ is the Lambert W function (or product logarithm) and[3]

$$\gamma(z_2) = \frac{\Delta_{\mathbf{PZ}}(\vartheta(\alpha^*))z_2 - v^*}{v^*}. \tag{56}$$

Moreover, for the hybrid system $\mathscr{H}_{R,\mathrm{FA}}^{(\alpha^*,\varepsilon)}$ with initial condition $(\theta_0, \dot{\theta}_0) = (\Phi_{\mathbf{PZ}}(z_1^-(\alpha^*)), \Psi_{\mathbf{PZ}}(z_1^-(\alpha^*))z_2)$, the time to impact function is given by $T_I(\theta_0, \dot{\theta}_0) = T_{\mathbf{PZ}}(z_2)$ and the solution to the continuous dynamics (33) *is given by:*

$$\begin{bmatrix} \theta(t, \alpha^*) \\ \dot{\theta}(t, \alpha^*) \end{bmatrix} = \begin{bmatrix} \Phi_{\mathbf{PZ}}(z_1(t, \alpha^*)) \\ \Psi_{\mathbf{PZ}}(z_1(t, \alpha^*))z_2(t, \alpha^*) \end{bmatrix} \tag{57}$$

for $0 \le t \le T_I(\theta_0, \dot{\theta}_0)$.

Proof: For $z_2 \in S_R \cap \mathbf{PZ}_{\alpha^*}$, the corresponding initial condition for the partial hybrid zero dynamics is given by the pre-impact point $(z_1^-(\alpha^*), z_2)$. Correspondingly, applying the reset map to this point for the partial hybrid zero dynamics (43) yields the initial condition $(z_1^+(\alpha^*), \Delta_{\mathbf{PZ}}(\vartheta(\alpha^*))z_2)$ for the partial zero dynamics (42) with solution given by (53). According to the definition of the guard for the partial hybrid zero dynamics (46), to establish that $T_{\mathbf{PZ}}(z_2)$ is the time-to-impact function it is necessary to determine the time, t^*, such that $z_1(t^*, \alpha^*) = z_1^-(\alpha^*)$. It is easy to verify through direct calculation that solving for t^* yields $t^* = T_{\mathbf{PZ}}(z_2)$ as desired.

The fact that the solution to $\mathscr{H}_{R,\mathrm{FA}}^{(\alpha^*,\varepsilon)}$ is given by (57) for the given initial condition follows from $\Delta_R(S_R \cap \mathbf{PZ}_{\alpha^*}) \subset \mathbf{PZ}_{\alpha^*}$. In particular, the system evolves according to the partial hybrid zero dynamics (42) with solution given by (53). By the definition of $\mathbf{PZ}_{\alpha^*}$, it follows that (41) can be used to obtain $(\theta(t), \dot{\theta}(t))$ from $(z_1(t, \alpha^*), z_2(t, \alpha^*)$ for all $0 \le t \le T_{\mathbf{PZ}}(z_2) = T_I(\theta_0, \dot{\theta}_0)$. ∎

Main Fully Actuated Result. The main result of this paper, in the context of full actuation, is that the point $(\vartheta(\alpha^*), \dot{\vartheta}(\alpha^*))$, determined through the inverse kinematics and utilizing the parameters obtained by solving the optimization problem in Theorem 1, is "essentially" the fixed point to a stable hybrid periodic orbit. Thus, the constrained optimization problem (HIO) not only ensures partial hybrid zero dynamics, but it automatically yields a fixed point to a stable walking gait that can be computed in closed form from the parameters of the human-inspired controller. Moreover, since the cost function (19) only depends on human walking data, we automatically generate a controller for a stable walking gait, its parameters, a stable hybrid periodic orbit and its fixed point using only human data.

Theorem 2: *Let α^* be the parameters solving* (HIO)*. If $\tau(\vartheta(\alpha^*)) > 0$ then there exists a constant $\bar{\varepsilon} > 0$ such that for all $\varepsilon > \bar{\varepsilon}$ the hybrid system $\mathscr{H}_{R,\mathrm{FA}}^{(\alpha^*,\varepsilon)}$ has an exponentially stable periodic orbit, $\mathscr{O}_\varepsilon$, dependent on ε, with fixed point $(\theta_\varepsilon^*, \dot{\theta}_\varepsilon^*) \in S$ and period T_ε which satisfy the following properties:*

$$\lim_{\varepsilon\to\infty} T_\varepsilon = \tau(\vartheta(\alpha^*)) \tag{P1}$$

$$\lim_{\varepsilon\to\infty} (\theta_\varepsilon^*, \dot{\theta}_\varepsilon^*) = (\vartheta(\alpha^*), \dot{\vartheta}(\alpha^*)) \tag{P2}$$

$$\lim_{\varepsilon\to\infty} \mathscr{O}_\varepsilon = \left\{ \begin{bmatrix} \Phi_{\mathbf{PZ}}(\hat{z}_1(t, \alpha^*)) \\ \Phi_{\mathbf{PZ}}(\hat{z}_1(t, \alpha^*))v^* \end{bmatrix} : 0 \le t \le \tau(\vartheta(\alpha^*)) \right\} \tag{P3}$$

where $\hat{z}_1(t, \alpha^*) = v^*t + y_1^H(\Delta_\theta\vartheta(\alpha^*))$.

Proof: From the constructions related to Proposition 1, the Poincaré map (45) can be explicitly computed; in fact, it is given by (55). To see this, for $z_2 \in S_R \cap \mathbf{PZ}_\alpha$, it is given by

$$\begin{aligned} \rho_\varepsilon(z_2) &= v^* + e^{-T_{\mathbf{PZ}}(z_2)\varepsilon}(\Delta_{\mathbf{PZ}}(\vartheta(\alpha^*))z_2 - v^*) \\ &= v^*\left(1 + \mathcal{W}\left(e^{-\varepsilon\tau(\vartheta(\alpha^*))}e^{\gamma(z_2)}\gamma(z_2)\right)\right) \end{aligned}$$

with $T_{\mathbf{PZ}}(z_2)$ and $\gamma(z_2)$ given in (54) and (56), respectivly. From the explicit form of the reduced Poincaré map ρ_ε it follows that:

$$\lim_{\varepsilon\to\infty} \rho_\varepsilon(z_2) = v^* = z_2^-(\alpha^*) \tag{58}$$

since $W(0) = 0$ and $\tau(\vartheta(\alpha^*)) > 0$.

To prove the existence of a periodic orbit for the partial hybrid zero dynamics, we need only prove the existence of a fixed point for ρ_ε. Consider a ball of radius $\delta > 0$ around v^*, i.e., for $z_2 \in B_\delta(v^*)$, $|z_2 - v^*| < \delta$. Then for this δ it follows by (58) that there exists a $\varepsilon_1 > 0$ such that for all $\varepsilon > \varepsilon_1$, $|\rho_\varepsilon(z_2) - v^*| < \delta$. Therefore, $\rho_\varepsilon : B_\delta(v^*) \to B_\delta(v^*)$. By the Brouwer fixed-point theorem, it follows that there exists a fixed point of ρ_ε, i.e., $z_2^*(\varepsilon)$, dependent on ε and satisfying $\rho_\varepsilon(z_2^*(\varepsilon)) = z_2^*(\varepsilon)$, and the hybrid partial zero dynamics has a periodic orbit. To prove the stability of this periodic orbit, we need only check the derivative of ρ_ε at $z_2^*(\varepsilon)$ and ensure that its magnitude is less than 1. The derivative ρ_ε can be explicitly computed as:

$$\rho_\varepsilon'(z_2^*(\varepsilon)) = \begin{cases} e^{-\varepsilon\tau(\vartheta(\alpha^*))}\Delta_{\mathbf{PZ}}(\vartheta(\alpha^*)) & \text{if} \quad z_2^*(\varepsilon) = v^* \\ \frac{\Delta_{\mathbf{PZ}}(\vartheta(\alpha^*))^2(z_2^*(\varepsilon) - v^*)}{\Delta_{\mathbf{PZ}}(\vartheta(\alpha^*))z_2^*(\varepsilon) - v^*} & \text{otherwise} \end{cases}$$

[3]Note that γ determines the change in the (linearized) velocity of the hip relative to v^*; or, in other words, the perturbation away from the full zero dynamics surface $\mathbf{FZ}_\alpha$. That is, if we were to require the stronger condition of full hybrid zero dynamics, $\Delta_R(S_R \cap \mathbf{FZ}_\alpha) \subset \mathbf{FZ}_\alpha$, then $\gamma(z_2) = 0$ from which it would follow that $T_{\mathbf{PZ}}(z_2) = \tau(\vartheta(\alpha^*))$.

Since $z_2^*(\varepsilon) \to v^* = z_2^-(\alpha^*)$ as $\varepsilon \to \infty$, it follows that

$$\lim_{\varepsilon \to 0} \rho_\varepsilon'(z_2^*(\varepsilon)) = 0.$$

Therefore, there exists an $\varepsilon_2 > 0$ such that for $\varepsilon > \varepsilon_2$, $|\rho_\varepsilon'(z_2^*(\varepsilon))| < 1$ establishing the stability of the periodic orbit for the partial hybrid zero dynamics.

To establish the existence of a stable periodic orbit O_ε for $\mathscr{H}_{R,\mathrm{FA}}^{(\alpha^*,\varepsilon)}$, by Theorem 4.5 of [51] (see also [30]) a stable fixed point for the restricted Poincaré map ρ_ε implies that:

$$(\theta_\varepsilon^*, \dot\theta_\varepsilon^*) = (\Phi_{\mathbf{PZ}}(z_1(\alpha^*)), \Psi_{\mathbf{PZ}}(z_1(\alpha^*))z_2^*(\varepsilon)) \tag{59}$$

is a stable fixed point of the Poincaré map P_ε for the hybrid system $\mathscr{H}_{R,\mathrm{FA}}^{(\alpha^*,\varepsilon)}$ for ε sufficiently large, i.e., for $\varepsilon > \varepsilon_3$. Picking $\bar\varepsilon = \max\{\varepsilon_1, \varepsilon_2, \varepsilon_3\}$ implies the desired existence and stability result.

To complete the proof, note that (P1)-(P3) follow from Proposition 1 applied to $z_2^*(\varepsilon)$. In particular, inspection of (54) yields (P1). Since $\lim_{\varepsilon\to\infty} z_2^*(\varepsilon) = z_2^-(\alpha^*)$, (P2) follows from (59) since $(\vartheta(\alpha^*), \dot\vartheta(\alpha^*)) = (\Phi_{\mathbf{PZ}}(z_1(\alpha^*)), \Psi_{\mathbf{PZ}}(z_1(\alpha^*))z_2^-(\alpha^*))$. Finally, (P3) follows from the fact that for the initial condition $(\theta_\varepsilon^*, \dot\theta_\varepsilon^*)$ the periodic orbit is defined by (57) with $z_2 = z_2^*(\varepsilon)$. Using (P1) coupled with the fact that, from (53), $\lim_{\varepsilon\to\infty} z_1(t,\alpha^*) = \hat z_1(t,\alpha^*)$ and $\lim_{\varepsilon\to\infty} z_2(t,\alpha^*) = v^*$ yields the desired result. ■

Imposing Physical Realizability Constraints. Thoerem 2 demonstrated that partial hybrid zero dynamics implies the existance of a stable periodic orbit that can be completley characterized in the limit. Yet, for the purposes of realization on physical robots, convergence is often not enough; it is desirable to know, in closed form, the solution of the system so that constraints on physical realizability can imposed directly in the optimization in closed form (e.g., constraints on maximum torque, foot height, etc.). The importance of Proposition 1, in addition to the role it played in proving Theorem 2, is that it allows for these conditions to be enforced in closed form. To provide a specific example, suppose that the maximum allowable torque by the motors is $u_{\max}$. For a given $\varepsilon > 0$ we can enforce this constraint by solving for $z_2^*(\varepsilon)$ such that $\rho_\varepsilon(z_2^*(\varepsilon)) = z_2^*(\varepsilon)$. Using $z_2^*(\varepsilon)$ in Proposition 1, through (57) the periodic solution $(\theta(t,\alpha^*), \dot\theta(t,\alpha^*))$ to the hybrid system $\mathscr{H}_{R,\mathrm{FA}}^{(\alpha^*,\varepsilon)}$ can be constructed in closed form, resulting in the constraint:

$$\max_{0\le t\le T_{\mathbf{PZ}}(z_2^*(\varepsilon))} \|u_{\mathrm{FA}}^{(\alpha,\varepsilon)}(\theta(t,\alpha^*), \dot\theta(t,\alpha^*))\|_\infty < u_{\max} \tag{C4}$$

which, when added to (HIO), will ensure that the maximum allowable torque is not violated (assuming a feasible solution to the optimization problem is found). The same approach can be utilized to implement constraints on maximum power, angular velocity, minimum foot height (i.e., scuffing prevention) and ZMP conditions. In essence, any behavior that can be quantified in terms of the solution to the dynamics can be codified in closed form through the closed form solution obtained from partial hybrid zero dynamics via Proposition 1.

Simulation Results. It will now be demonstrated how these formal results can be applied to models of bipedal robots, and specifically AMBER and NAO, to achieve walking in simulation. These simulation results serve as the basis for the control of the actual NAO robot to obtain walking experimentally as will be discussed at the end of this section.

AMBER: We begin with the hybrid model of AMBER, $\mathscr{H}_{R,\mathrm{FA}}^{(\alpha^*,\varepsilon)}$, obtained using the mass, length and inertia values of this robot (in this case, we assume the robot is fully actuated for the sake of simulation only—we later consider the more physically realistic case of underactuation). Utilizing the human output combination specified in (11)-(15) and the associated human output data, we numerically solve the optimization problem in Theorem 1. In particular, we utilize only the human data (for the cost in (HIO)), and seed the optimization problem with the parameters of the canonical walking functions that best fit the human output data (as given in Table I). The end result of this optimization are parameters α^* for the human-inspired controller that provably result in stable robotic walking due to Theorem 2, along with the initial condition to this walking gait: $(\vartheta(\alpha), \dot\vartheta(\alpha))$.

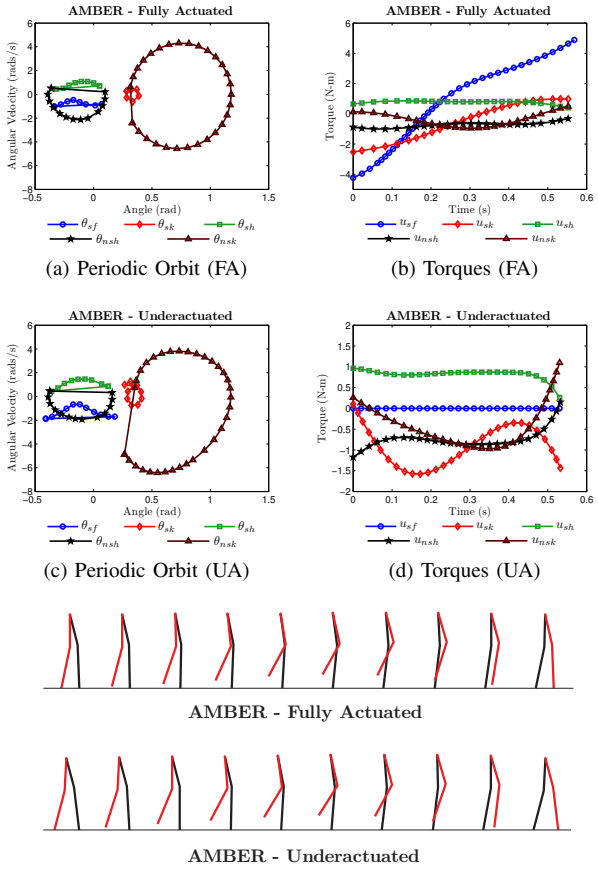

(a) Periodic Orbit (FA) (b) Torques (FA)

(c) Periodic Orbit (UA) (d) Torques (UA)

Fig. 6: The walking gaits for AMBER in the case of both full (left) and under (right) actuation. The periodic orbits corresponding to the walking gaits are shown in (a) for the fully actuated case and (c) for the underactuated case. Similarly, the torques for the fully and under actuated case are shown in (b) and (d).

Comparing the parameters of the human-inspired controller, and thus the canonical walking functions, obtained as a result of Theorem 1 against the mean human walking data (see Fig. 5) it can be seen that the resulting robotic walking is in fact "human-like." In particular, in [34], "normal" human walking is defined to be walking that lies within one standard deviation of mean human walking. In the case of the considered outputs, the walking for AMBER lies almost entirely within this one standard deviation band indicating "normal" human walking. The one exception is the velocity of the hip which is modulated to take into account the physical differences between AMBER the humans from which the data was collected. The walking gait obtained, as simulated from the initial condition $(\vartheta(\alpha^*), \dot\vartheta(\alpha^*))$ with $\varepsilon = 20$, can be seen in Fig. 6, with the corresponding periodic orbit and torques required shown in Fig. 6(a),(b). While Theorem 2 formally guarantees stability of the periodic orbit, we verify this numerically by computing the eigenvalues of the Poincaré map; we find the largest magnitude of an eigenvalue to be 0.0172, indicating

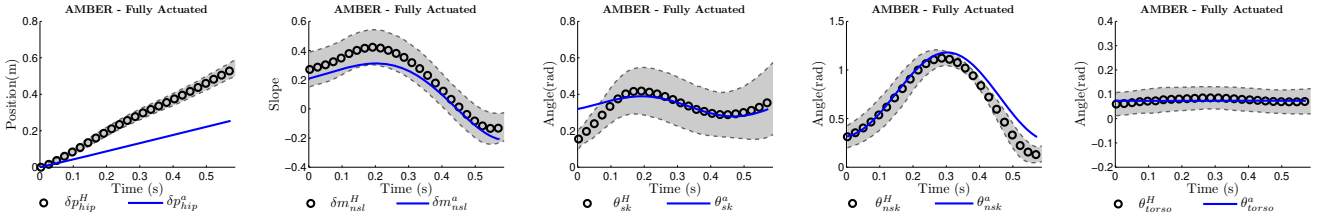

(a) Human Outputs and Outputs for AMBER for Fully Actuated Walking

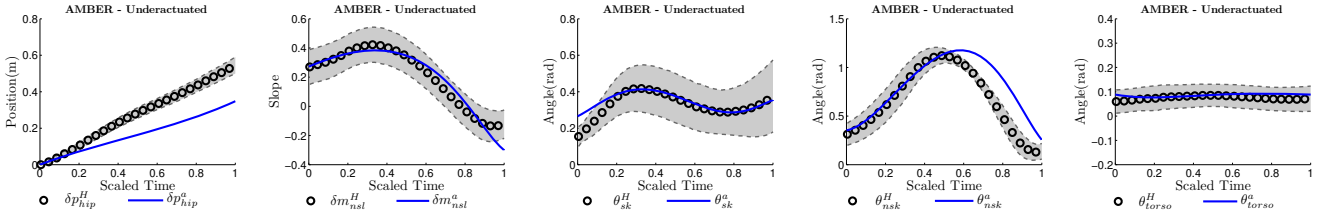

(b) Human Outputs and Outputs for AMBER for Underactuated Walking

Fig. 5: The outputs of AMBER (blue) for fully actuated (a) and underactuated (b) walking obtained plotted against the mean human output data computed from the data of nine subjects walking, with error bands showing one standard deviation from the mean.

local exponential stability (in fact, all other eigenvalues are essentially zero as the proof of Theorem 2 predicts).

NAO: We apply Theorem 1 to the hybrid model of NAO where, to achieve practical results (with a view towards implementation), additional constraints were enforced in this optimization which limited the maximum joint velocity to 3 rad/s and ensured proper foot clearance. The end result is parameters α^* for the human-inspired controller that (due to Theorem 2) result in stable robotic walking for sufficiently large control gain ε. Picking $\varepsilon = 25$ and simulating the hybrid system $\mathscr{H}_{R,\mathrm{FA}}^{(\alpha^*,\varepsilon)}$ (with the mass, lengths and inertia values for NAO) from the initial condition $(\vartheta(\alpha^*), \dot{\vartheta}(\alpha^*))$ verifies that we do, in fact, have a walking gait, i.e., a periodic orbit (see Fig. 7(b),(e)). Moreover, we can verify the fact that the chosen ε results in a stable walking gait by checking the eigenvalues of the Poincaré map; we find that the magnitude of the maximum eigenvalue is $\lambda = 0.1059$, thus verifying the exponential stability guaranteed by Theorem 2. Furthermore, and as indicated in Fig. 7(c), the resulting walking exhibits partial hybrid zero dynamics. In addition to stable, periodic walking, the robustness of the human-inspired control law allows for the robot to start from rest and converge to the walking periodic orbit corresponding to the walking gait. As shown in Fig. 7(a), trajectories of the system when started from rest converge to the stable limit periodic orbit predicted by Theorem 2. Convergence is also seen in a plot of the human inspired outputs; in Fig. 7(c) the convergence of the actual outputs of the robot to the desired outputs can be seen. Tiles of the first step of the walking, starting from rest, can be seen in Fig. 7(d). These simulated trajectories will be used to experimentally achieve walking on the real NAO robot.

NAO Experimental Results. Implementing the simulated trajectories of the human-inspired walking control on NAO results in dynamically stable walking on the actual NAO robot. In particular, the simulated trajectories, starting from rest, are implemented on the sagittal actuators of the robot through trajectory tracking, and a simple feedback control law is implemented in the lateral plane (more details can be found in [7]). Tiles of the walking gait achieved on the NAO robot can be seen in Fig. 9 where the experimental walking is compared to tiles of the simulated walking taken at the same time instances showing that, in fact, there is good agreement. To provide qualitative evidence of this, the simulated and experimentally observed figures are plotted in Fig. 10 where very good agreement between simulation and experimentation is shown. Finally, the human-inspired walking that was obtained on NAO subjectively appears more human-like than other walking gaits that have been achieved for NAO through ZMP related methods [25], [48]. We invite readers to form their own opinion by watching the video [4] of the human-inspired robotic walking and its comparison with the pre-existing (ZMP) walking.

VI. Human-Inspired Hybrid Zero Dynamics

Having demonstrated how human-inspired control automatically results in "human-like" robotic walking for fully actuated bipedal robots, this section shows how robotic walking is also automatically obtained from human data in the case of underactuation. In particular, we now consider *hybrid zero dynamics* (HZD) as originally developed for the underatuated control of bipedal robots [19], [51]. In the framework of HZD, we add constraints to the human-inspired optimization in Theorem 1 so that the parameters that guarantee HZD also imply the existence of a stable walking gait for an underactuated robot. Moreover, we can explicitly compute the fixed point to the stable periodic orbit corresponding to this stable walking gait.

Problem Statement. The goal of the underactuated human-inspired controller (34) is to drive the outputs of the robot to the outputs of the human: $y_{a,2} \to y_{d,2}$. In other words, the controller renders the *zero dynamics surface*:

$$\mathbf{Z}_\alpha = \{(\theta, \dot{\theta}) \in T\mathcal{Q}_R : y_2(\theta) = \mathbf{0},\ L_{f_R} y_2(\theta, \dot{\theta}) = \mathbf{0}\} \tag{60}$$

exponentially stable; moreover, this surface is invariant for the continuous dynamics of the hybrid system $\mathscr{H}_{R,\mathrm{UA}}^{(\alpha,\varepsilon)}$ defined in (35). Note that the hybrid zero dynamics surface is simply the partial hybrid zero dynamics surface, $\mathbf{PZ}$, considered in the case of full actuation; that is, for underactuation $\mathbf{PZ} = \mathbf{Z}$, and this was one of the original motivations for considering the partial hybrid zero dynamics surface. As in the case of full actuation, the goal of *human-inspired HZD* is to find parameters α^* that solve the following constrained optimization problem:

$$\alpha^* = \underset{\alpha \in \mathbb{R}^{21}}{\operatorname{argmin}}\ \mathrm{Cost}_{\mathrm{HD}}(\alpha) \tag{61}$$

$$\text{s.t} \quad \Delta_R(S_R \cap \mathbf{Z}_\alpha) \subset \mathbf{Z}_\alpha \tag{HZD}$$

with $\mathrm{Cost}_{\mathrm{HD}}$ the cost given in (19). The formal goal of this section is to restate (PHZD) in such a way that it can be practically solved through the utilization of the constructions for the fully actuated case, but suitably modified for underactuation.

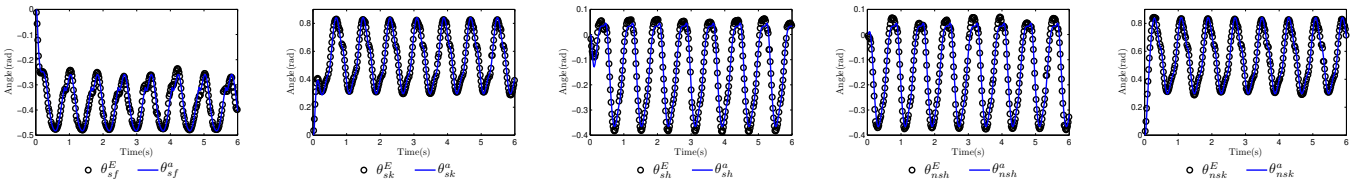

(a) Stance Ankle (b) Stance Knee (c) Stance Hip (d) Non-stance Hip (e) Non-stance knee

Fig. 8: Simulated (desired) and experimental joint trajectories in the sagittal plane for NAO.

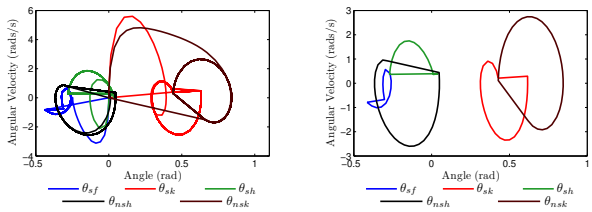

(a) Periodic Orbit from Rest (b) Periodic Orbit from Fixed Point

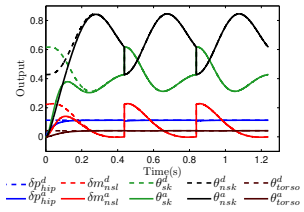

(c) Outputs from Rest

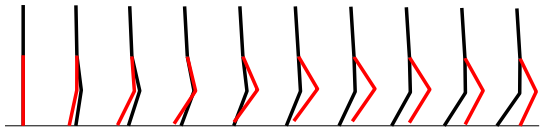

(d) Gait Tiles from Rest

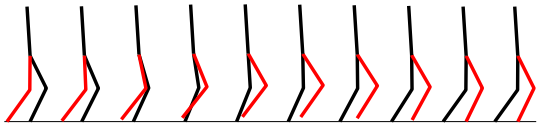

(e) Gait Tiles from Fixed Point

Fig. 7: Periodic orbits for the simulated behavior of NAO starting from rest, i.e., a zero initial condition (a) and the fixed point of the periodic orbit (b). Starting from rest, the actual outputs of NAO converge to the desired outputs and display partial hybrid zero dynamics (c). Snapshots of the walking gaits from the NAO simulation starting from zero initial conditions (d) and continuing from the fixed point (e).

Zero Dynamics. The zero dynamics must be constructed so as to take into account the fact that the system is underactuated. In particular, the zero dynamics will no longer be linear as in the case of full actuation. To this end we will utilize the constructions in [51], reframed in the context of canonical walking functions. Because of the specific choice of $y_{a,2}$ in (22), we begin by picking the following coordinates for the zero dynamics:

$$\begin{aligned} \xi_1 &= y_1^H(\theta) =: c\theta \\ \xi_2 &= D(\theta)_{1,*}\dot{\theta} =: \gamma_0(\theta)\dot{\theta} \end{aligned} \tag{62}$$

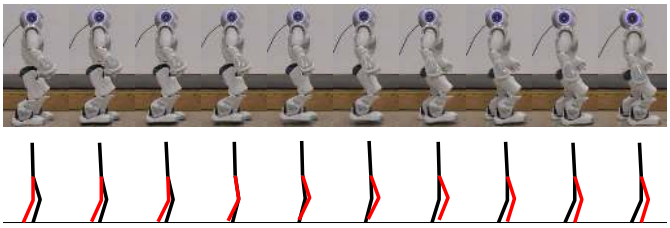

Fig. 9: Simulated (desired) and experimental joint trajectories for the sagittal plane (a). Comparison of the actual (top) and simulated (bottom) walking gaits for NAO over one step (b).

where $D(\theta)_{1,*}$ is the first row of the inertia matrix in (4). Moreover, as in the case of full actuation, we can again write $y_{d,2}(\xi_1) = y_{d,2}(\tau(\theta))$.

Picking the coordinates η_1 and η_2 as in (40) and defining

$$\begin{aligned} \Phi_{\mathbf{Z}}(\xi_1) &= \begin{bmatrix} c \\ H \end{bmatrix}^{-1} \begin{pmatrix} \xi_1 \\ y_{d,2}(\xi_1) \end{pmatrix} \\ \Psi_{\mathbf{Z}}(\xi_1) &= \begin{bmatrix} \gamma_0(\Phi_{\mathbf{Z}}(\xi_1)) \\ H - \frac{\partial y_{d,2}(\xi_1)}{\partial \xi_1} c \end{bmatrix}^{-1} \begin{pmatrix} 1 \\ 0 \end{pmatrix} \end{aligned}$$

it follows that for $\theta = \Phi_{\mathbf{Z}}(\xi_1)$ and $\dot{\theta} = \Psi_{\mathbf{Z}}(\xi_1)\xi_2$ that $(\theta, \dot{\theta}) \in \mathbf{Z}_\alpha$. Finally, the zero dynamics evolve according to the ODE:

$$\begin{aligned} \dot{\xi}_1 &= \kappa_1(\xi_1)\xi_2 & \kappa_1(\xi_1) &:= c\Psi_{\mathbf{Z}}(\xi_1) \\ \dot{\xi}_2 &= \kappa_2(\xi_1) & \kappa_2(\xi_1) &:= \left.\frac{\partial V(\theta)}{\partial \theta_{sf}}\right|_{\theta=\Phi_{\mathbf{Z}}(\xi_1)} \end{aligned} \tag{63}$$

with V the potential energy of the robot (4).

The advantage of the low-dimensional zero dynamic representation introduced is that it allows for the existence and stability of a fixed point of the zero dynamics to be determined *a priori*. In the case of underactuation, this is achieved by considering the energy of the zero dynamics, and in particular the potential energy. As in the case with full actuation, we begin with a point on the guard $(\theta^-, \dot{\theta}^-) \in S_R$ with its post-impact state $(\theta^+, \dot{\theta}^+) = \Delta_R(\theta^-, \dot{\theta}^-)$, we can compute $\xi_1^- = y_1^H(\theta^-)$ and $\xi_1^+ = y_1^H(\theta^+)$. From this, the change in ξ_2 due to this impact can be determined through:

$$\Delta_{\mathbf{Z}}(\theta^-) = \gamma_0(\theta^+)\Delta_{\dot{\theta}}(\theta^-)\Psi_{\mathbf{Z}}(y_1^H(\theta^-)) \tag{64}$$

wherein $\xi_2^+ = \Delta_{\mathbf{Z}}(\theta^-)\xi_2^-$.

Picking the same Poincaré section as in the case of full actuation (46), the stability of a periodic orbit can be characterized by 1-dimensional discrete time dynamical system $\rho : S_R \cap \mathbf{Z}_\alpha \to S_R \cap \mathbf{Z}_\alpha$, given by:

$$\xi_2[k+1] = \rho(\xi_2[k]) = \Delta_{\mathbf{Z}}(\theta^-)\xi_2[k] - V_{\mathbf{Z}}(y_1^H(\theta^-))$$

where

$$V_{\mathbf{Z}}(\xi_1) := -\int_{\xi_1^+}^{\xi_1} \frac{\kappa_2(\xi)}{\kappa_1(\xi)} d\xi.$$

is the potential energy of the zero dynamics (63). Energy methods can be coupled with these constructions to determine when the robot will take a step by considering the constant:

$$\mathscr{D}_{\mathbf{Z}}(\theta^-) = \frac{\Delta_{\mathbf{Z}}(\theta^-)^2}{1-\Delta_{\mathbf{Z}}(\theta^-)^2} V_{\mathbf{Z}}(y_1^H(\theta^-)) + V_{\mathbf{Z}}^{\max}$$

with $V_{\mathbf{Z}}^{\max} = \max_{\xi_1^+ \leq \xi \leq \xi_1^-} V_{\mathbf{Z}}(\xi)$. Specifically, if $\mathscr{D}_{\mathbf{Z}}(\theta^-) < 0$ it will imply the existence of a limit cycle in the hybrid zero dynamics surface, and if $0 < \Delta_{\mathbf{Z}}(\theta^-) < 1$ it will imply the stability of that limit cycle [51].

Main Underactuated Result. We now present the main result of this paper related to underactuated walking. Picking $\vartheta(\alpha)$ and $\dot{\vartheta}(\alpha)$ (see (47) and (50)) as the choice of $(\theta^-, \dot{\theta}^-)$ constraints can be added to the human-inspired optimization problem (HIO) to automatically obtain an initial condition corresponding to stable periodic walking for an underactuated robot.

Theorem 3: *The parameters α^* solving the constrained optimization problem* (HIO) *in Theorem 1 subject to the additional constraints:*

$$\mathscr{D}_{\mathbf{Z}}(\vartheta(\alpha)) < 0 \tag{C4}$$
$$0 < \Delta_{\mathbf{Z}}(\vartheta(\alpha)) < 1 \tag{C5}$$

yields hybrid zero dynamics: $\Delta_R(S_R \cap \mathbf{Z}_{\alpha^*}) \subset \mathbf{Z}_{\alpha^*}$. Moreover, there exists an $\hat{\varepsilon} > 0$ such that for all $\varepsilon > \hat{\varepsilon}$ the hybrid system $\mathscr{H}_{R,\mathrm{UA}}^{(\alpha^*,\varepsilon)}$ has a stable periodic orbit with fixed point $(\theta^*, \dot{\theta}^*) \in S_R \cap \mathbf{Z}_{\alpha^*}$ given by:

$$\theta^* = \vartheta(\alpha), \quad \dot{\theta}^* = \Psi_{\mathbf{Z}}(c\vartheta(\alpha)) \left(-\sqrt{\frac{-V_{\mathbf{Z}}(\vartheta(\alpha))}{1-\Delta_{\mathbf{Z}}(\vartheta(\alpha))}} \right).$$

Proof: From Theorem 1, it follows that conditions (C1)-(C3) imply partial hybrid zero dynamics. Since in the case of underactuation $\mathbf{PZ} = \mathbf{Z}$ and $\mathbf{FZ} \subset \mathbf{Z}$ it follows that these conditions imply hybrid zero dynamics: $\Delta_R(S_R \cap \mathbf{Z}_{\alpha^*}) \subset \mathbf{Z}_{\alpha^*}$. Utilizing Theorem 5.3 in [51], conditions (C4) and (C5) imply the desired result. ■

Simulation Results. Since AMBER (Fig. 1) is an underactuated robot due to its point feet, we apply the results of this section to AMBER to obtain underactuated human-inspired robotic walking in simulation. We will then discuss how this simulated walking can be used as a basis for the controller design on the physical bipedal robot with the end result being real-world robotic walking.

We begin with the application of Theorem 3 to the underactuated hybrid model of AMBER. Specifically, we solve the optimization problem in Theorem 1 subject to the additional constraints in Theorem 3. The end result of this optimization is a collection of control parameters for the α^* resulting in a hybrid system $\mathscr{H}_{R,\mathrm{UA}}^{(\alpha^*,\varepsilon)}$. Moreover, the same optimization automatically generates a fixed point to a stable periodic orbit (shown in Fig. 6(c)); this is verified by picking $\varepsilon = 10$ and checking the eigenvalues of the linearization of the Poincaré map for which the maximum magnitude is 0.7761 (and hence less than 1). Tiles of the walking obtained in simulation can be seen in Fig. 6. In addition, it can be seen in Fig. 6(d) that the walking is very low torque (in fact, the torque is far lower than for the fully actuated walking obtained). What is especially interesting is the comparison of the outputs, $y_{a,2}$, of the robot against the human output data as shown in Fig. 5. Despite the fact that the robot consists of only 5 degrees of freedom and is underactuated at the ankle, the end result is still "human-like" walking–the outputs of robot fall within one standard deviation of the mean human data for a majority of the outputs.

Experimental Results. The underactuated walking obtained through simulation forms a basis for the controllers realized on the physical robot AMBER. The implementation details are involved (see [55]), and do not lie within the scope of this paper, but the matrix of parameters α^* is used as the control parameters for a voltage based feedback proportional controller that was also shown to obtain walking in simulation (shown in Fig. 11). Finally, this feedback voltage control was implemented on the physical robot through National Instruments CompactRIO system. The end result was human-inspired robotic walking as can be seen in Fig. 11. Good agreement between the simulated and experimental behavior was observed; for example, the simulated and experimental trajectories can be seen in Fig. 10. Note that the differences between these trajectories are a result of the fact that the simulated trajectories are not tracked directly, but rather feedback voltage control is used, which can result in drift. Nonetheless, the end result of this approach is "human-like" robotic walking; this can best be seen by watching the actual walking which can be found at [2]. Even more interesting is that this human-inspired walking appears to be very robust. As can be seen at [2], the robot AMBER is subjected to disturbances both on the robot and as a result of the environment. The robot is able to react to these disturbances in such a way that walking is maintained and, more subjectively, AMBER reacts in a "human-like" manner.

We argue that the robust walking behavior seen on AMBER is a result of the strong human motivation for the controller design. In particular, this gives direct evidence for the benefits of considering the canonical walking function: its introduces compliant behavior into

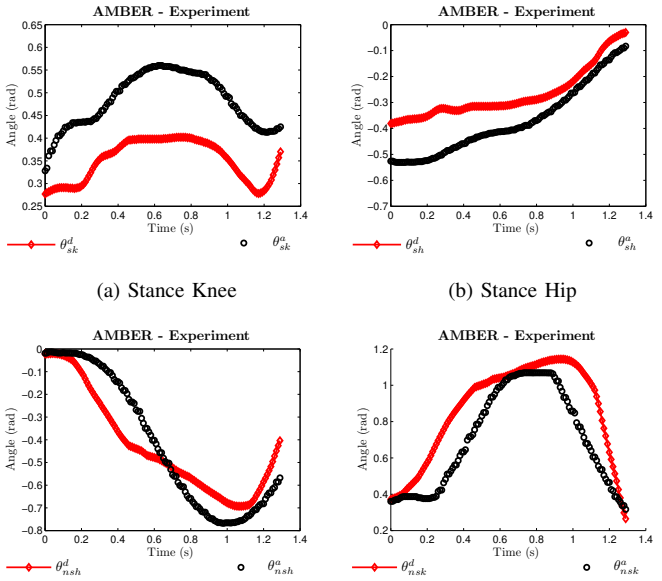

(a) Stance Knee (b) Stance Hip

(c) Non-stance Hip (d) Non-stance knee

Fig. 10: Simulated (desired) and experimental joint trajectories for AMBER.

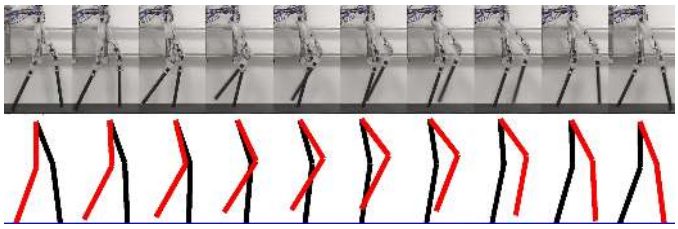

Fig. 11: Comparison of the simulated and experimental walking gait for AMBER over one step.

system even if this is not present in their mechanical design, and the form of the functions result in more robust behavior outside of the region for which they are defined. In support of the first point, it can be seen in [2] that when AMBER walks over obstacles it reacts in a compliant fashion at the knee. This is due to the spring-damper nature functions underlying human control. In a related fashion, when operating outside of its original behavior (flat ground walking), i.e., when the system is being disturbed, it again acts in a natural way. This is in contrast to control methods which rely on polynomials as a basis for control, since polynomial functions typically only have well-defined behavior in the interval for which they are defined. Canonical walking functions display reasonable behavior outside of the region for which they are defined due to the sinusoidal and exponential terms coupled with the small number of parameters. We argue that these factors combine to potentially imply that something intrinsic to human walking may be present in human-inspired control.

VII. Conclusions

This paper presents a formal human-inspired approach to bipedal robotic walking, proving through Theorem 1, 2 and 3 that by using only human data, parameters to the human-inspired controller can be determined that simultaneously: provide the best fit of the human data, yield (partial) hybrid zero dynamics, imply the existence of a stable walking gait, and allow the fixed point for this stable walking gait to be explicitly computed. Moreover, these results are established in the case of both full and under actuation. To demonstrate these results, walking gaits are generated in simulation for two models of bipedal robots: AMBER and NAO. In the case of AMBER, both full and under actuated walking is achieved that is remarkably "human-like." In the case of NAO, the robustness of the walking obtained through human-inspired control allows for both steady state walking and walking starting from rest. Finally, the formal results presented are utilized to achieve robotic walking in experimentation on both AMBER in NAO. In particular, 3D fully actuated bipedal robotic walking is obtained for NAO, and 2D underactuated bipedal robotic walking is achieved with AMBER. This provides evidence of the practical applicability of the formal results presented in this paper. This hope is, therefore, that these results lay the groundwork for a "human-inspired" framework for robotic locomotion controller design.

Acknowledgements. I would like to thank the members of AMBER Lab for their contributions in developing the framework of human-inspired control and their essential work in experimentally realizing the formal results presented in this paper. I would also like to thank Jessy Grizzle for the many enlightening discussions on hybrid zero dynamics. Finally, I would like to thank the anonymous reviewers and the Associate Editor for their insightful and constructive comments on this manuscript.

References

[1] http://www.aldebaran-robotics.com/.

[2] "First human-inspired robotic walking with AMBER," http://www.youtube.com/watch?v=SYXWoNU8QUE.

[3] "First human-inspired robotic walking with AMBER 2.0," http://www.youtube.com/watch?v=Ih9gNmzbm1A.

[4] "First human-inspired robotic walking with NAO," http://www.youtube.com/watch?v=OBGHU-e1kc0.

[5] A. D. Ames, "First steps toward automatically generating bipedal robotic walking from human data," in *Robotic Motion and Control 2011*, ser. LNICS, vol. 422. Springer, 2012, pp. 89–116.

[6] ——, "First steps toward underactuated human-inspired bipedal robotic walking," in *IEEE International Conference on Robotics and Automation*, St. Paul, MN, 2012.

[7] A. D. Ames, E. A. Cousineau, and M. J. Powell, "Dynamically stable robotic walking with NAO via human-inspired hybrid zero dynamics," in *Hybrid Systems: Computation and Control*, Beijing, 2012.

[8] A. D. Ames, R. D. Gregg, and M. W. Spong, "A geometric approach to three-dimensional hipped bipedal robotic walking," in *45th Conference on Decision and Control*, San Diago, CA, 2007.

[9] A. D. Ames, R. Vasudevan, and R. Bajcsy, "Human-data based cost of bipedal robotic walking," in *Hybrid Systems: Computation and Control*, Chicago, IL, 2011.

[10] I. Beloozerova and M. Sirota, "The role of the motor cortex in the control of accuracy of locomotor movements in the cat," *J. Physiol (Lond)*, vol. 461, pp. 1–25, 1993.

[11] D. J. Braun and M. Goldfarb, "A control approach for actuated dynamic walking in bipedal robots," *IEEE TRO*, vol. 25, no. 6, pp. 1292–1303, Dec. 2009.

[12] C. Chevallereau, G. Bessonnet, G. Abba, and Y. Aoustin, *Bipedal Robots: Modeling, Design and Walking Synthesis*. New York: Wiley-ISTE, Jan. 2009.

[13] C. Chevallereau, A. Formal'sky, and D. Djoudi, "Tracking a joint path for the walk of an underactuated biped," *Robotica*, vol. 22, no. 1, pp. 15–28, Jan. 2004.

[14] S. Collins and A. Ruina, "A bipedal walking robot with efficient and human-like gait," Apr. 2005.

[15] T. Drew, "Motor cortical activity during voluntary gait modifications in the cat I. cells related to the forelimbs," *J. Neurophysiology*, vol. 70, no. 1, pp. 179–199, 1993.

[16] B. Espiau and A. Goswami, "Compass gait revisited," in *IFAC Symposium on Robot Control*, Capri, Sep. 1994, pp. 839–846.

[17] A. Goswami, B. Thuilot, and B. Espiau, "A study of the passive gait of a compass-like biped robot: Symmetry and chaos," *IJRR*, vol. 17, no. 12, pp. 1282–1301, Dec. 1998.

[18] M. Goulding, "Circuits controlling vertebrate locomotion: moving in a new direction," *Annu Rev Neurosci.*, vol. 10, no. 7, pp. 507–18, 2009.

[19] J. W. Grizzle, G. Abba, and F. Plestan, "Asymptotically stable walking for biped robots: Analysis via systems with impulse effects," *IEEE TAC*, vol. 46, no. 1, pp. 51–64, Jan. 2001.

[20] J. W. Grizzle, C. Chevallereau, A. D. Ames, and R. W. Sinnet, "3D bipedal robotic walking: models, feedback control, and open problems," in *IFAC Symposium on Nonlinear Control Systems*, Bologna, Sep. 2010.

[21] J. W. Grizzle, C. Chevallereau, and C. Shih, "Asymptotically stable walking of a five-link underactuated 3D bipedal robot," *IEEE Transactions on Robotics*, vol. 25, pp. 37–50, 2009.

[22] M. O. Heller, G. Bergmann, G. Deuretzbacher, L. Dürselen, M. Pohl, L. Claes, N. P. Haas, and G. N. Duda, "Musculo-skeletal loading conditions at the hip during walking and stair climbing," *J. of Biomechanics*, vol. 34, pp. 883–893, 2001.

[23] P. Holmes, R. J. Full, D. Koditschek, and J. Guckenheimer, "The dynamics of legged locomotion: Models, analyses, and challenges," *SIAM Review*, vol. 48, no. 2, pp. 207–304, May 2006.

[24] Y. Hürmüzlü and D. B. Marghitu, "Rigid body collions of planar kinematic chains with multiple contact points," *Intl. J. of Robotics Research*, vol. 13, no. 1, pp. 82–92, Feb. 1994.

[25] S. Kajita, F. Kanehiro, K. Kaneko, K. Fujiwara, K. Harada, K. Yokoi, and H. Hirukawa, "Biped walking pattern generation by using preview control of zero-moment point," in *IEEE - International Conference on Robotics and Automoation*, Taipei, 2003, pp. 1620–1626.

[26] O. Kiehn, "Locomotor circuits in the mammalian spinal cord," *Annu Rev Neurosci.*, vol. 29, pp. 279–306, 2006.

[27] D. Koepl and J. W. Hurst, "Force control for planar spring-mass running," in *IEEE International Conference on Intelligent Robots and Systems (IROS)*, 2011.

[28] A. D. Kuo, "Energetics of actively powered locomotion using the simplest walking model," *Journal of Biomechanical Engineering*, vol. 124, pp. 113–120, 2002.

[29] T. McGeer, "Passive dynamic walking," *Intl. J. of Robotics Research*, vol. 9, no. 2, pp. 62–82, Apr. 1990.

[30] B. Morris and J. Grizzle, "A restricted Poincaré map for determining exponentially stable periodic orbits in systems with impulse effects: Application to bipedal robots," in *IEEE Conf. on Decision and Control*, Seville, Spain, December 2005.

[31] R. M. Murray, Z. Li, and S. S. Sastry, *A Mathematical Introduction to Robotic Manipulation*. Boca Raton: CRC Press, Mar. 1994.

[32] V. M.Zatsiorsky, *Kinematics of Human Motion*, 1st ed. Champaign: Human Kinetics, Sep. 1997.

[33] M. Pasupuleti, S. N. Yadukumar, and A. D. Ames, "Human-inspired underactuated bipedal robotic walking with amber on flat-ground, up-

slope and uneven terrain," in *IEEE/RSJ International Conference on Intelligent Robots and Systems (IROS)*, Vilamoura, Algarve, 2012.
[34] J. Perry and J. Burnfield, *Gait Analysis: Normal and Pathological Function*, 2nd ed. Thorofare: Slack Incorporated, 2010.
[35] I. Poulakakis and J. W. Grizzle, "The spring loaded inverted pendulum as the hybrid zero dynamics of an asymmetric hopper," *IEEE TAC*, vol. 54, no. 8, pp. 1779–93, Aug. 2009.
[36] M. Powell, A. Hereid, and A. D. Ames, "Speed regulation in 3D robotic walking through motion transitions between human-inspired partial hybrid zero dynamics," submitted to the IEEE International Conference on Robotics and Automation, 2013.
[37] M. J. Powell, H. Zhao, and A. D. Ames, "Motion primitives for human-inspired bipedal robotic locomotion: Walking and stair climbing," in *IEEE International Conference on Robotics and Automation*, St. Paul, MN, 2012.
[38] J. Rose and J. G. Gamble, *Human Walking*. Philadelphia: Lippincott Williams & Wilkins, Dec. 2005.
[39] S. S. Sastry, *Nonlinear Systems: Analysis, Stability and Control*. New York: Springer, Jun. 1999.
[40] T. Schaub, M. Scheint, M. Sobotka, W. Seiberl, and M. Buss, "Effects of compliant ankles on bipedal locomotion," in *EEE/RSJ Intl. Conf. on Intelligent Robots and Systems*, 2009.
[41] R. W. Sinnet and A. D. Ames, "3D bipedal walking with knees and feet: A hybrid geometric approach," in *48th IEEE Conference on Decision and Control*, Shanghai, P.R. China, 2009.
[42] R. W. Sinnet, S. Jiang, and A. D. Ames, "A human-inspired framework for bipedal robotic walking design," to appear in the International Journal of Biomechatronics and Biomedical Robotics, 2013.
[43] R. W. Sinnet, M. J. Powell, S. Jiang, and A. D. Ames, "Compass gait revisited: A human data perspective with extensions to three dimensions," in *50th IEEE Conference on Decision and Control and European Control Conference.*, 2011.
[44] M. W. Spong and F. Bullo, "Controlled symmetries and passive walking," *IEEE TAC*, vol. 50, no. 7, pp. 1025–1031, 2005.
[45] S. Srinivasan, I. A. Raptis, and E. R. Westervelt, "Low-dimensional sagittal plane model of normal human walking," *ASME J. of Biomechanical Eng.*, vol. 130, no. 5, Oct. 2008.
[46] S. Srinivasan, E. Westervelt, and A. Hansen, "A low-dimensional sagittal-plane forward-dynamic model for asymmetric gait and its application to study the gait of transtibial prosthesis users," *ASME J. of Biomech. Eng.*, vol. 131, 2009.
[47] R. Vasudevan, A. D. Ames, and R. Bajcsy, "Using persistent homology to determine a human-data based cost for bipedal walking," in *18th IFAC World Congress*, Milan, Italy, 2011.
[48] M. Vukobratović and B. Borovac, "Zero-moment point—thirty-five years of its life," *Intl. J. of Humanoid Robotics*, vol. 1, no. 1, pp. 157–173, mar 2005.
[49] M. Vukobratović, B. Borovac, D. Surla, and D. Stokic, *Biped Locomotion*. Berlin: Springer-Verlag, Mar. 1990.
[50] E. Wendel and A. D. Ames, "Rank properties of Poincaré maps for hybrid systems with applications to bipedal walking," in *Hybrid Systems: Computation and Control*, Stockholm, Sweden, 2010.
[51] E. R. Westervelt, J. W. Grizzle, C. Chevallereau, J. H. Choi, and B. Morris, *Feedback Control of Dynamic Bipedal Robot Locomotion*. Boca Raton: CRC Press, Jun. 2007.
[52] D. A. Winter, *Biomechanics and Motor Control of Human Movement*, 2nd ed. New York: Wiley-Interscience, May 1990.
[53] Y. Xiang, J. Arora, H.-J. Chung, H.-J. Kwon, S. Rahmatalla, R. Bhatt, and K. Abdel-Malek, "Predictive simulation of human walking transitions using an optimization formulation," *Structural and Multidisciplinary Optimization*, pp. 1–14.
[54] S. N. Yadukuma, J. Lack, H. Zhao, W. Ma, and A. D. Ames, "Bipedal robotic walking with AMBER2 via human-inspired voltage control," submitted to the IEEE International Conference on Robotics and Automation, 2013.
[55] S. N. Yadukumar, M. Pasupuleti, and A. D. Ames, "From formal methods to algorithmic implementation of human inspired control on bipedal robots," in *Tenth International Workshop on the Algorithmic Foundations of Robotics (WAFR)*, Boston, MA, 2012.
[56] H. Zhao, S. N. Yadukumar, and A. D. Ames, "Bipedal robotic running with partial hybrid zero dynamics and human-inspired optimization," in *IEEE/RSJ International Conference on Intelligent Robots and Systems (IROS)*, Vilamoura, Algarve, 2012.